Medicago truncatula CORYNE regulates inflorescence meristem branching, nutrient signaling, and arbuscular mycorrhizal symbiosis

Johnathan Orosz[1], Erica Xinlei Lin[1]*, Penelope Lindsay[2]*, Mikayla Kappes[3], Sagar Bashyal[1,3,4], Hasani Everett[1], Chandan Kumar Gautam[1], David Jackson[2], Lena Maria Müller[1,3#]

* equal contribution

[#] corresponding author

[1]Department of Biology, University of Miami, Coral Gables, FL, USA

[2]Cold Spring Harbor Laboratory, Cold Spring Harbor, NY, USA

[3]The Salk Institute for Biological Studies, La Jolla, CA, USA

[4]School of Biological Sciences, University of California San Diego, La Jolla, CA 92093

Present addresses:

E.X.L.: Stowers Institute for Medical Research, Kansas City, MO 64110

H.E.: Systems, Synthetic, and Physical Biology, Rice University, Houston, TX 77005

C.K.G.: Department of Microbiological Sciences, North Dakota State University, Fargo, ND 58108

Abstract

The CLAVATA signaling pathway regulates plant development and plant-environment interactions. CLAVATA signaling consists of mobile, cell-type or environment-specific CLAVATA3/ESR-related (CLE) peptides, which are perceived by a receptor complex consisting of leucine-rich repeat receptor-like kinases such as CLAVATA1 and receptor-like proteins such as CLAVATA2, which often functions with the pseudokinase CORYNE (CRN). CLAVATA signaling has been extensively studied in various plant species for its role in meristem maintenance and in legumes for modulating root interactions with nitrogen-fixing rhizobia. Some signaling proteins involved in development and nodulation, including CLAVATA1, also regulate plant interactions with mutualistic arbuscular mycorrhizal (AM) fungi. However, our knowledge on AM symbiosis

regulation by CLAVATA signaling remains limited and only a handful of genetic regulators have been identified. Here we report that *Medicago truncatula CRN* controls inflorescence meristem branching and negatively regulates root interactions with AM fungi. *MtCRN* functions partially independently of the AM autoregulation signal *MtCLE53*. Transcriptomic data revealed that *crn* roots display signs of perturbed signaling related to a range of responses to biotic and abiotic factors, suggesting that *MtCRN* plays various roles in plant development and interactions with the environment.

Introduction

Cell-cell communication is critical for plant development and cellular responses to internal and external cues. CLAVATA (CLV) signaling, which consists of mobile CLAVATA3/ESR-related (CLE) peptide hormones and CLE receptor complexes, regulates many aspects of plant development and responses to the environment (Bashyal *et al.*, 2023; Lindsay *et al.*, 2023). CLE receptor complexes consist of leucine-rich repeat receptor-like kinases (LRR-RLKs) with an extracellular LRR ligand-binding domain and an intracellular kinase domain (e.g., CLAVATA1, CLV1, or BARELY ANY MERISTEM, BAM1-3), receptor-like proteins (e.g., CLAVATA2, CLV2) containing an extracellular ligand-binding domain but lack a kinase domain, and intracellular regulators like the membrane-bound pseudokinase CORYNE (CRN) (Hazak and Hardtke, 2016). In Arabidopsis and maize, CLV2 and CRN are considered a CLE perception unit (Bleckmann *et al.*, 2009; Je *et al.*, 2018). CLV2-CRN can form complexes with CLV1 or BAMs, but also function independently as a parallel pathway (Guo *et al.*, 2010; Somssich *et al.*, 2016*b*; Hazak *et al.*, 2017). Similarly, the *Medicago truncatula* ortholog of CLV1 (termed SUNN in this species), MtCLV2 and MtCRN can interact with each other (Crook *et al.*, 2016). While the cellular function of CRN is still elusive, co-expression assays in *Nicotiana benthamiana* leaves suggest that the short extracellular domain of AtCRN is important for stabilizing the CRN-CLV2 complex at the plasma membrane, whereas the intracellular kinase domain is important for transmitting CLE peptide signals (Somssich *et al.*, 2016*a*).

58 Mutations in CLV receptors and ligands disrupt meristem organization, often leading to enlarged
59 vegetative, inflorescence and floral shoot meristems (Lindsay *et al.*, 2023). These meristem
60 defects in turn impact floral organization and fruit development, altering the number of flowers
61 produced in an inflorescence, the number of floral organs that are produced, or the
62 arrangement and size of the fruit. The impact of a particular CLV mutation on meristem
63 organization depends on the specific gene mutated, the nature of the mutation (allele), and the
64 plant species; this phenomenon is thought to be a result of differences in compensatory
65 mechanisms in meristem maintenance among plant species (Rodriguez-Leal *et al.*, 2019). To
66 date, maize and Arabidopsis are the only plant species in which *crn* mutants have been
67 described. In both species, shoot and inflorescence meristems are enlarged. Arabiopsis *crn*
68 mutants produce more carpels per flower, and some flowers make stamens without anthers
69 (Müller *et al.*, 2008). Depending on the temperature, *crn* floral primordia and flowers are
70 prematurely terminated (Jones *et al.*, 2021). Maize *crn* mutants produce fasciated ears, with a
71 disordered arrangement of kernel rows and larger kernel row number (Je *et al.*, 2018). CLV
72 signaling also plays roles in root development, including maintenance of the root apical
73 meristem and protophloem differentiation. *AtCRN* is expressed in multiple cell types in the root,
74 including stele, endodermis, and quiescent center cells of the meristem (Somssich *et al.*, 2016*a*;
75 Hazak *et al.*, 2017). Phloem-expressed AtCRN was shown to be required for the perception of
76 root-active CLE peptides (Hazak *et al.*, 2017). Despite its importance for CLE signaling not all
77 Arabidopsis *crn* mutant alleles show a phenotype characterized by longer primary roots (Müller
78 *et al.*, 2008; Somssich *et al.*, 2016*a*; Hazak *et al.*, 2017), suggesting *CRN* by itself is not required
79 for root development.
80
81 In addition to plant development, CLAVATA signaling pathways also modulate plant interactions
82 with the environment, which includes responses to abiotic and biotic factors such as host
83 responses to pathogenic or beneficial microbes (Bashyal *et al.*, 2023). Mutualistic plant
84 interactions with rhizobia during nodulation or *Glomeromycotina* fungi during arbuscular
85 mycorrhiza (AM) symbiosis are regulated by various receptor-ligand signaling pathways (Roy and
86 Müller, 2022), including CLV signaling. In both symbioses, the host plant provides microbial

87 symbionts with photosynthetically fixed carbon in exchange for mineral nutrients. While
88 rhizobia supply the host with nitrogen (N), AM fungi provide a range of benefits including N,
89 phosphorus (P), and water (Smith and Reid, 2008). Both symbioses are governed by negative
90 regulatory pathways based on plant nutrient (N or P) status and prior microbial colonization
91 (autoregulation); these pathways are mediated by nutrient- or symbiosis-induced CLE peptides,
92 respectively (Roy and Müller, 2022). Autoregulation of nodulation (AON) is a systemic negative
93 feedback loop that has been studied in numerous legume species (Wang *et al.*, 2018). In *M.*
94 *truncatula*, AON is regulated by root-derived, nodule-induced CLE peptides (MtCLE12,
95 MtCLE13), which negatively regulate nodule number in a MtSUNN- and MtCRN-dependent
96 manner (Schnabel *et al.*, 2005; Crook *et al.*, 2016; Nowak *et al.*, 2019). Grafting experiments
97 revealed that MtSUNN and MtCRN act in the shoot (Schnabel *et al.*, 2005; Crook *et al.*, 2016);
98 however, both genes are also expressed in roots (Schnabel *et al.*, 2012; Crook *et al.*, 2016),
99 suggesting various functions across tissues and organs. Autoregulation of mycorrhizal symbiosis
100 (AOM) is regulated by the CLE peptide MtCLE53, which is induced in the vascular tissue of
101 colonized roots and negatively regulates AM fungal colonization by repressing biosynthesis of
102 strigolactones (Müller *et al.*, 2019; Karlo *et al.*, 2020, Preprint). Strigolactones are produced by
103 host plants in response to P and N starvation and promote AM symbiosis (Yoneyama *et al.*,
104 2007; Liu *et al.*, 2011; Foo *et al.*, 2013; Marro *et al.*, 2022). In the current AOM model, AM-
105 induced *MtCLE53* down-regulates strigolactone biosynthesis and consequently reduces
106 subsequent AM fungal root colonization (Müller *et al.*, 2019).
107
108 Like AON, AOM depends on the LRR-RLK SUNN. Plants defective in *SUNN* display a
109 hypermycorrhizal phenotype with elevated root colonization levels and arbuscule numbers and
110 are insensitive to *MtCLE53* overexpression (Morandi *et al.*, 2000; Müller *et al.*, 2019; Karlo *et al.*,
111 2020, Preprint). Despite many similarities, AOM is less understood than AON. Although AON
112 and AOM signal through the same LRR-RLK SUNN, the upstream-acting CLE peptides and
113 downstream signaling appear to at least partially differ between the two symbioses (Mortier *et*
114 *al.*, 2010; Müller *et al.*, 2019; Karlo *et al.*, 2020, Preprint; Chaulagain *et al.*, 2023*b*,*a*).
115 Furthermore, recent evidence from tomato (*Solanum lycopersicum*) suggests that AM symbiosis

116 is regulated by multiple, at least partially independent CLV signaling pathways: grafting
117 experiments revealed that while SlFAB (ortholog of CLV1) acts in the root, SlCLV2 is part of two
118 distinct signaling pathways controlling AM symbiosis from the shoot and the root, respectively
119 (Wang *et al.*, 2021). In addition, the AM-induced SlCLE11 peptide acts as a negative regulator of
120 AM symbiosis but functions independently of SlFAB or SlCLV2 (Wulf *et al.*, 2024). By contrast,
121 supernodulating pea mutants in *CLV2* (*sym28*), did not show a hypermycorrhizal phenotype,
122 suggesting species-specific differences in symbiosis regulation (Morandi *et al.*, 2000). In
123 addition, in contrast to *MtCLE53* over-expression, *sunn* itself (as well as mutants in the tomato
124 and pea orthologs) does not exhibit mis-regulated strigolactone biosynthesis (Foo *et al.*, 2014;
125 Müller *et al.*, 2019; Karlo *et al.*, 2020, Preprint; Wang *et al.*, 2021), suggesting additional
126 signaling components must be involved in MtCLE53-SUNN-mediated AOM signaling that impact
127 strigolactone biosynthesis.
128
129 In addition to autoregulation, AM symbiosis is tightly regulated by the availability of soil mineral
130 nutrients to the plant. High N or P concentrations in the substrate can suppress AM symbiosis
131 development (Abbott *et al.*, 1984). Although P is the predominant element plants acquire
132 through AM fungi, N starvation can promote AM symbiosis even under high P (Nouri *et al.*,
133 2014). In *M. truncatula*, P-induced *MtCLE33* acts as a negative regulator of AM symbiosis via a
134 SUNN-dependent pathway although SUNN itself is not required for P repression of AM
135 symbiosis (Müller *et al.*, 2019). Similarly, work in tomato revealed that regulation of AM by CLV
136 receptors is independent of P but depends on plant N status (Wang *et al.*, 2021). Despite
137 substantial progress in recent years, our knowledge on AM symbiosis regulation by CLV signaling
138 is incomplete and fragmented across plant species. Similar to meristem development, CLV
139 signaling may be differently wired across plant species with different nutrient uptake strategies
140 and capacities for symbiotic interactions.
141
142 Here, we report *MtCRN* as a regulator of *M. truncatula* inflorescence branching. In addition, we
143 find that *MtCRN* acts as a negative regulator of AM symbiosis in *M. truncatula*. Our results
144 further suggest that, while *MtCRN* contributes to AOM, it also regulates AM symbiosis via

145 additional pathways. Transcriptomics data suggest that *crn* mutants display broad alterations in
146 response to biotic and abiotic factors, indicating that MtCRN may integrate multiple signaling
147 pathways with distinct outcomes.
148
149 **Results**
150
151 ***M. truncatula* CLAVATA signaling regulates inflorescence meristem branching and flowering**
152 **time but is dispensable for root development**
153 Mutants in CLV signaling have previously been described to be impaired in meristem
154 maintenance, with mutants often displaying inflorescence or stem fasciation (Clark *et al.*, 1997).
155 Arabidopsis *CRN* specifically has been reported to modulate inflorescence meristem termination
156 and flower outgrowth under stress (Müller *et al.*, 2008; Jones *et al.*, 2021). Although legume CLV
157 mutants have been extensively studied in the context of plant-microbe symbioses, reports on
158 developmental phenotypes are rare. Notable exceptions are pea *sym28* mutants, which display
159 stem fasciation and produce excess leaves and flowers per node (Krusell *et al.*, 2011), and
160 *GmCLV1A*, which regulates shoot branching as well as flower number and development, and
161 appears to have functionally diversified from its symbiosis-regulating paralog *GmNARK* (Mirzaei
162 *et al.*, 2017).
163
164 To understand if CLV signaling is also involved in shoot development of other legumes, we
165 investigated above-ground developmental phenotypes of *M. truncatula* mutants carrying a
166 homozygous Tnt1 insertion within the coding sequence of the pseudokinase *MtCRN* (Crook *et*
167 *al.*, 2016). Above-ground development, including time to flowering, appeared to be delayed in
168 *crn* when compared to R108 wild-types (Supplementary Fig.1). Stem fasciation, which is
169 characteristic for many CLV pathway mutants in other species (Somssich *et al.*, 2016*b*), was not
170 observed. *M. truncatula* typically produces one solitary flower per inflorescence unit (Fig. 1A, B)
171 (Benlloch *et al.*, 2003). However, we noted that *crn* mutants displayed two flowers per peduncle
172 with high frequency: 91% of 8-week old *crn* (n= 11 inflorescences) produced two flowers (often
173 with an additional third bud appearing from the same inflorescence, Fig. 1C, D, Supplementary

174 Fig. 1), whereas R108 wildtype plants of the same age and grown under the same growth
175 conditions only produced a single flower per peduncle (n=14 inflorescences, Fig. 1A, B,
176 Supplementary Fig. 1). Notably, similar inflorescence phenotypes (76% of inflorescences, n=25)
177 were detected in *M. truncatula* mutants defective in the *CLV1* ortholog *SUNN* (*sunn-5*;
178 Supplementary Fig. 1), suggesting both *SUNN* and *MtCRN* regulate inflorescence meristem
179 branching. Although *crn* mutants produced two flowers per peduncle, ultimately only a single
180 seed was produced per inflorescence as one of the two flowers typically appeared to terminate
181 prematurely. In Arabidopsis, *crn* mutants show increased numbers of floral organs and
182 increased inflorescence meristem size (Müller *et al.*, 2008). However, manual dissection of
183 flowers as well as scanning electron microscopy analysis of inflorescences revealed that floral
184 organ numbers and inflorescence width of *M. truncatula crn* did not differ from those in R108
185 wildtypes (Figure 1 A-G). This indicates that, unlike Arabidopsis and maize, meristem branching
186 rather than stem cell proliferation is altered in *M. truncatula crn*.
187
188 In roots, CLV signaling is critical for root meristem maintenance, lateral root emergence, and
189 protophloem differentiation (Hazak and Hardtke, 2016). We set out to investigate if *M.*
190 *truncatula crn* mutants play a role in root development by analyzing root system architecture of
191 12-day old *crn* and R108 seedlings grown on agar plates. *M. truncatula crn* mutants did not
192 display strong defects in root system development in our experimental growth conditions. We
193 did not detect differences in primary root length, lateral root number, lateral root length, or
194 lateral root density (lateral roots per cm primary root length) between *crn* and R108
195 (Supplementary Figure 1). This is reminiscent of the phenotypes previously reported in
196 Arabidopsis, where *crn* mutants do not show altered root development although *CRN* is
197 required for the perception of root-active CLE peptides (Müller *et al.*, 2008; Hazak *et al.*, 2017).
198
199 ***MtCRN* negatively regulates AM symbiosis**
200 *M. truncatula* CRN was previously described as a negative regulator of nodulation symbiosis in
201 concert with SUNN (Crook *et al.*, 2016; Nowak *et al.*, 2019). AON, AOM, and nutrient regulation
202 of AM symbiosis share multiple common components, including CLV1, but the role of CRN in

203 AM symbiosis regulation has not been investigated. Because tomato *clv2* mutants are
204 hypermycorrhizal (Wang *et al.*, 2018), CRN-CLV2 are commonly considered a signaling unit
205 (Müller *et al.*, 2008), and MtCRN can interact with the AOM regulator SUNN as well as MtCLV2
206 (Crook *et al.*, 2016), we hypothesized that *MtCRN* may also regulate root interactions with AM
207 fungi. Indeed, *crn* mutants displayed significantly increased overall *R. irregularis* root
208 colonization levels relative to the R108 wildtype (Figure 2A). A detailed analysis revealed that
209 *crn* mutants also show higher arbuscule density (i.e., number of arbuscules per mm colonized
210 root in a defined region at the hyphopodium) than wildtype roots, whereas vesicle density
211 (vesicles/mm colonized roots) did not differ between the wild-type and the mutant (Figure 2B-
212 E). These results are consistent with the hypothesis that MtCRN acts as a negative regulator of
213 AM symbiosis.
214
215 ***MtCRN* functions partially independent of the AOM signal MtCLE53**
216 Autoregulation of nodulation (AON) and mycorrhizal symbiosis (AOM) negatively regulates
217 nodulation and AM symbiosis, respectively, based on existing symbioses. *MtCRN* has been
218 implicated in AON and acts downstream of the nodulation-induced CLE peptides MtCLE12 and
219 MtCLE13 (Nowak *et al.*, 2019). We previously reported that ectopic over-expression of the *M.*
220 *truncatula* AOM signal *MtCLE53* reduced overall root length colonization in a SUNN-dependent
221 manner (Müller *et al.*, 2019). To test if *MtCRN* also acts down-stream of AOM signals, we over-
222 expressed *MtCLE53* under the control of the constitutively active Cauliflower mosaic virus 35S
223 promoter (*35S::MtCLE53*) as well as a control construct (*35S::GUS*) in roots of *crn* mutants and
224 R108 wild-type controls. Similar to what was previously reported for the *M. truncatula* A17
225 accession (Müller *et al.*, 2019; Karlo *et al.*, 2020, Preprint), ectopic over-expression of *MtCLE53*
226 roots also reduced overall AM fungal root length colonization in R108. Interestingly, unlike *sunn*,
227 which is fully insensitive to *MtCLE53* over-expression suggesting the LRR-RLK acts in the same
228 pathway as the peptide hormone (Müller *et al.*, 2019), ectopic *MtCLE53* overexpression reduced
229 AM fungal root length colonization also in *crn* (Fig. 3). However, colonization reduction in
230 *35S::MtCLE53* relative to *35S::GUS*-expressing roots is weaker in *crn* (29%) than in the wild-type
231 background (41%). The partial sensitivity of *crn* to *MtCLE53* over-expression suggests that

232 *MtCRN* is involved in *MtCLE53* signaling but that the AM symbiosis phenotype of *crn* may also
233 be influenced by additional, *MtCLE53*-independent pathways.
234
235 **Transcriptomic analysis of *M. truncatula crn* mutants reveals global changes in stress**
236 **response, nutrient homeostasis, and environment interactions**
237 To understand the molecular mechanisms causing the elevated AM fungal root colonization
238 levels in *crn* mutants, we sequenced the transcriptomes of 3 *R. irregularis*-colonized and 4
239 mock-inoculated *crn* and R108 wild-type root systems, respectively (Supplementary table 1). As
240 expected, we observed major transcriptomic changes induced by *R. irregularis* colonization in
241 R108 wild-type roots (434 up-regulated and 266 down-regulated genes, here defined as
242 differentially expressed genes with a log2 fold-change >1 or <-1, respectively, and padj<0.05;
243 Supplementary figure 2, Supplementary figure 3). Comparing *R. irregularis*-colonized *crn* mutant
244 roots with mock-inoculated *crn* roots, we identified 816 up- and 325-downregulated genes
245 (Supplementary figure 2, Supplementary figure 4). In mock-inoculated *crn* roots relative to
246 mock-inoculated wild-type roots, we identified 1506 up- and 647 down-regulated genes
247 (Supplementary figure 2, Supplementary figure 5). When comparing differentially expressed
248 genes in *R. irregularis*-colonized *crn* roots with *R. irregularis*-colonized wild-type roots, we
249 identified 1061 up- and 594-downregulated genes (Supplementary figure 2, Supplementary
250 figure 6, Supplementary table 2). Because *crn* roots are more colonized than wild-type roots,
251 these observed transcriptomic differences may be caused by genotype differences and/or
252 differences in AM fungal colonization levels. We performed hierarchical clustering analysis of all
253 differentially expressed genes in *R. irregularis*-inoculated *crn* roots relative to *R. irregularis*-
254 inoculated wild-type roots to identify clusters of differentially expressed genes with similar
255 expression patterns and to distinguish differentially expressed genes solely influenced by
256 colonization levels from those regulated by *MtCRN*.
257
258 Differentially expressed genes were grouped into 6 clusters (Fig. 4A, Supplementary table 2).
259 Clusters 1, 3 and 6 contained genes that are regulated by AM fungal root colonization, and
260 whose general expression pattern changes were similar in *crn* and wild-type roots. However, the

261 degree of up- or down-regulation differs between the genotypes, likely caused by the
262 differential colonization levels in the mutant compared to the wildtype (Fig. 2 A-E).
263
264 Cluster 1 genes are induced by AM symbiosis and are generally more highly expressed in *R.*
265 *irregularis*-colonized *crn* roots relative to colonized wild-type roots (Fig. 4A). GO analysis of the
266 genes in cluster 1 revealed, among others, an enrichment of genes associated with GO terms
267 related to symbiosis ("AM association", "response to symbiotic fungus", "nodulation"), nitrate
268 assimilation, as well as genes associated with the biosynthesis and transport of secondary
269 metabolites and hormones known to regulate AM symbiosis (e.g., carotenoids, gibberellic acid,
270 brassinosteroids; Fig. 4B, Supplementary table 3). This cluster contains well-studied AM marker
271 genes including but not limited to *MtPT4*, *MtRAM1*, *MtRAM2,* or *MtSTR*, which function in
272 bidirectional nutrient exchange between the symbiotic partner and whose expression is known
273 to be correlated with AM colonization levels (Serrano *et al.*, 2024).
274
275 Clusters 3 and 6 contain genes that are down-regulated by AM fungal root colonization; AM-
276 mediated down-regulation is more pronounced in *crn* roots than in wildtypes. While no
277 significant GO terms were found in cluster 3 (11 genes), in cluster 6 we detected enrichment of
278 GO terms related to cell wall biogenesis and remodeling (Fig. 4D, Supplementary table 3) as well
279 as ethylene signaling. Notably, this GO term contained 5 transcription factors of the
280 APETALA2/ETHYLENE RESPONSE FACTOR (AP2/ERF) family; however, AP2/ERF transcription
281 factors have a more role in plant stress signaling, and, apart from ethylene, also often respond
282 to the hormones abscisic acid (ABA), gibberellic acid (GA), brassinosteroids (BR), and cytokinin
283 (Xie *et al.*, 2019). To our knowledge, no symbiosis-related function has been reported for any of
284 the AP2/ERF transcription factors in cluster 6.
285
286 Cluster 2 contains 549 genes that are up-regulated in *crn* roots relative to wild-type roots,
287 regardless of AMF colonization status (Fig. 4A). Many genes in this cluster appear to play roles in
288 plant responses to abiotic and biotic stresses: The GO term with the highest fold-enrichment
289 (61-fold) in this cluster is saponin biosynthetic process (Fig. 4C, Supplementary table 3).

290 Saponins are secondary metabolites with antioxidant activity that play various roles in plant-
291 microbe interactions, including plant defense against pathogens and herbivores (Mugford and
292 Osbourn, 2012; Chen *et al.*, 2014). Soy saponins have been identified in root exudates as
293 modulators of plant interactions with rhizosphere microbes (Tsuno *et al.*, 2018; Fujimatsu *et al.*,
294 2020). In addition, 12 peroxidases associated with the GO terms "hydrogen peroxide catabolic
295 process" and "cellular oxidant detoxification" were enriched in cluster 2. Peroxidases are major
296 regulators of cellular reactive oxygen species (ROS) homeostasis (Passardi *et al.*, 2005). ROS play
297 various roles in plants, including response to pathogens and beneficial microbes, including AM,
298 but also development, signaling, and cell growth (Wojtaszek, 1997; Fester and Hause, 2005;
299 Huang *et al.*, 2019). The GO term "cellular modified amino acid metabolic process" was
300 enriched in cluster 2; this GO term contained (among others) 4 genes annotated as glutathione
301 S-transferases, which also have antioxidant activity and are involved in ROS scavenging and
302 cellular detoxification during stress responses (Gullner *et al.*, 2018). Together, this data suggests
303 that cellular oxidative stress may be attenuated in *crn* through increased ROS scavenging.
304 Conversely, *crn* roots display an enrichment of GO terms associated with lipid metabolism ("lipid
305 biosynthetic process", "fatty acid metabolic process", "monocarboxylic acid biosynthetic
306 process") and oxylipin biosynthesis. The latter contained four genes encoding 9-lipoxigenases
307 (*9-LOX*), and one gene annotated as *ALPHA-DIOXYGENASE 1 (αDOX1)*. 9-oxylipins play a role in
308 cellular signaling, defense, and abiotic stress response (Vicente *et al.*, 2012), and their up-
309 regulation suggests that *crn* mutants may have a heightened response to biotic stress even in
310 the absence of microbes. In line with this hypothesis, the GO term "defense response" was also
311 enriched among the genes in cluster 2 (Fig. 4C); this GO term contained several genes encoding
312 NUCLEOTIDE-BINDING SITE LEUCINE-RICH REPEAT (NBS-LRR) family proteins, which can directly
313 bind to microbial effectors and thus play critical roles in plant immune responses to pathogens
314 (Marone *et al.*, 2013). This suggests that, despite signatures of attenuated oxidative stress,
315 other components of the plant response system to biotic stresses are up-regulated in *crn*.
316
317 Furthermore, we detected an enrichment of genes associated with the GO term
318 "transmembrane transport" among the *crn*-upregulated genes in cluster 2. Interestingly, these

319 included, among others, genes encoding transporters for carbon products such as sugar
320 (*MtESL16.1/MtESL2.4, MtESL3.4, MtESL6.4, MtSTP3.2, MtSTP5.1/MtSTP5.2*), which may
321 indicate that carbon flux is altered in *crn*. In addition, we identified putative transporters for
322 nitrate (*MtNPF2.11, MtNPF5.13, MtNPF5.5, MtNPF5.10*), ammonium (*Medtr4g017820*),
323 phosphate (*MtPT2, MtPT9*), metals (*MtMTP8*), potassium (*Medtr4g099260*), and zinc (*MtZIP6*)
324 among the genes in cluster 2 (Supplementary table 2, Supplementary table 3), suggesting mis-
325 regulation of various nutrient uptake or homeostasis pathways in the mutant (further discussed
326 below).
327
328 Cluster 4 contains genes that are down-regulated in *crn* roots relative to wild-type roots with
329 little impact of symbiosis status (Fig. 4A). In this group of 391 genes, only the GO term 'plant-
330 type secondary cell wall biogenesis' was enriched (Supplementary table 3). Intriguingly, all 13
331 genes associated with this GO term in cluster 4 are annotated as FASCICLIN-LIKE
332 ARABINOGALACTAN PROTEIN (FLA). FLAs are extracellular glycoproteins involved in a plethora
333 of functions, including development, growth, and environmental responses (He *et al.*, 2019),
334 but to our knowledge have not been studied in the context of AM symbiosis or CLAVATA
335 signaling. However, genes encoding arabinogalactan proteins as well as other cell wall-related
336 genes have been shown to be down-regulated also in a *A. thaliana crn* mutant (Pallakies and
337 Simon, 2014). This suggests a conserved role of CRN in cell wall organization, which is critical for
338 its function in growth and development.
339
340 Cluster 5 contains 14 genes that are induced in R108 *R. irregularis*-colonized roots relative to
341 mock-inoculated roots but show the opposite pattern in *crn* background (down-regulated in *R.*
342 *irregularis*-colonized roots relative to mock-inoculated *crn* roots) (Fig. 4A, Supplementary table
343 3). No significantly enriched GO terms were detected in cluster 5.
344
345 **N and P homeostasis signaling is perturbed in *crn* roots**
346 Our cluster analysis suggests an up-regulation of multiple mineral nutrient transporters in *crn*,
347 regardless of root colonization status (see above, Supplementary table 3). This suggests that in

348 *crn* mutants, nutrient starvation and/or homeostasis signaling pathways may be mis-regulated.
349 Because P and N are major regulators of AM symbiosis and their homeostasis is regulated by
350 CLAVATA signaling pathways in various plant species (Bashyal *et al.*, 2023), we examined genes
351 associated with P and N homeostasis more closely in our dataset. Interestingly, 16 genes
352 putatively associated with N homeostasis were regulated by *MtCRN* regardless of root
353 colonization status, and 11 additional ones were found to be synergistically regulated by *MtCRN*
354 and AM status of the plant (Fig. 5A-B, Supplementary table 4). Similarly, 8 genes associated with
355 P homeostasis were mis-regulated in *crn* relative to R108 without additional regulation by root
356 colonization status, and an additional 3 genes were regulated by *MtCRN* and AM symbiosis (Fig.
357 5C-D, Supplementary table 4). This data suggests a major perturbance in nutrient homeostasis
358 signaling in *crn* even in the absence of symbiosis. Because nutrient starving plants initiate more
359 interactions with beneficial microbes (Nouri *et al.*, 2014), a mis-regulation of nutrient
360 homeostasis and/or starvation signaling may promote AM fungal root colonization in *crn*.
361
362 **Expression of early symbiosis signaling genes is mis-regulated in *crn***
363 Consistent with an increase in AM fungal root colonization, we observed elevated gene
364 expression of known AM-induced genes in *R. irregularis*-colonized *crn* roots relative to colonized
365 wild-type controls (see above). This was the case for well-studied genes involved in arbuscule
366 accommodation and symbiotic nutrient exchange (e.g., *MtPT4*, *MtRAM2*, *MtSTR*), and arbuscule
367 degeneration (e.g., *MtMYB1*, *MtCP3*, *MtTGL*) (Figure 6A and B, Supplementary table 5).
368 Expression of these genes did not differ when mock-inoculated *crn* roots were compared to
369 mock-inoculated R108 roots.
370
371 Conversely, expression of many genes involved in pre-symbiotic signaling was perturbed in
372 mock-inoculated *crn* roots relative to mock-inoculated wildtype roots, suggesting these genes
373 may be direct or indirect targets of *MtCRN* signaling: We found that the expression of genes
374 involved in strigolactone biosynthesis and secretion (*MtD27*, *MtCCD7*, *MtCCD8*, *MtPDR1a*) not
375 only respond to AM fungal root colonization in *crn* and R108, but are also differentially
376 regulated in *crn* mock-inoculated roots relative to mock-inoculated wild-type controls (Fig. 6A

377 and B). In addition, *MtCCD8b* and *MtMAX1a*, orthologs of genes involved in strigolactone
378 biosynthesis in other species, as well as *MtMAX2* and *MtD14*, involved in strigolactone signaling
379 and perception, respond to AM fungal root colonization and are also differentially regulated in
380 mock-inoculated *crn* roots relative to controls. Similar trends were observed for the known
381 transcriptional regulators governing strigolactone biosynthesis *NSP1* and *NSP2.* Because the
382 production of AM-symbiosis promoting strigolactones is regulated by P and N status of the plant
383 (Yoneyama *et al.*, 2007, 2012; Liu *et al.*, 2011; Foo *et al.*, 2013; Marro *et al.*, 2022), an up-
384 regulation of the strigolactone biosynthesis pathway may be a consequence of the apparent
385 mis-regulation of N and P homeostasis signaling in *crn* roots (Fig. 5A-D).
386
387 In addition, expression of several genes involved in the common symbiosis signaling pathway
388 (CSSP) appear to be directly or indirectly regulated by *MtCRN* (Fig. 6A-B). The CSSP is triggered
389 by cellular perception of N-acetylglucosamine (GlcNAc)-derived (lipo)chitooligosaccharide
390 molecules derived from AM fungi or rhizobia (myc-LCOs/COs or nod-LCOs, respectively), and is
391 required for cellular entry of symbiotic microbes at the onset of symbiotic interactions (Oldroyd,
392 2013). *DMI2*, which encodes a putative co-receptor perceiving microbial signals, was found to
393 be up-regulated in mock-inoculated *crn* roots when compared to R108. Likewise, *DMI3*, *IPD3*,
394 and *VPY*, which regulate cellular signal transduction and symbiosis initiation in response to
395 microbial LCO perception (MacLean *et al.*, 2017; Lindsay *et al.*, 2022) function downstream of
396 *MtCRN* signaling. In addition, *DMI3* and *VPY* expression was also found to be responsive to AM
397 symbiosis (Fig. 6A). Because the CSSP pathway is not only required for the establishment of AM
398 but also nodulation symbiosis, and because *crn* was reported to have a hypermycorrhizal
399 phenotype (this study) and a hypernodulation phenotype in *M. truncatula* (Crook *et al.*, 2016),
400 we hypothesize that *crn* mutants are primed for symbiotic interactions even in the absence of
401 microbes, potentially due to an up-regulation of the symbiosis accommodation program as a
402 result of perturbations in N and P starvation signaling (Li *et al.*, 2022). In line with this
403 hypothesis, we found that some genes encoding lysin motif (LysM) RLKs involved in the
404 recognition of nod- and myc-LCOs (e.g., *MtLYK8* and *NFP*, but not *MtLYK3*) are up-regulated in
405 *crn* roots even in the absence of a microbe (Fig. 6 C-D, supplementary table 1, supplementary

406 table 6) (Limpens *et al.*, 2003; Smit *et al.*, 2007; Zhang *et al.*, 2024). Intriguingly, 10 additional
407 LysM RLKs or receptor-like proteins (LYK, LYR, LYM) that can bind LCOs but have no known role in
408 nodulation or symbiosis (Buendia *et al.*, 2018) were also up-regulated in *crn* mutants relative to
409 wildtypes (both in *R. irregularis*- or mock-inoculated treatments), suggesting recognition of
410 diverse microbial patterns may be altered in *crn*.
411
412 ***Rhizophagus irregularis* transcriptionally responds to colonizing *crn* roots**
413 To investigate R*. irregularis* responses to host genotype, we mapped our transcriptome reads to
414 the *R. irregularis* DAOM197198 v2.0 genome (Yildirir *et al.*, 2022). About 1.2-3.8 % of the reads
415 mapped to the fungal genome in colonized R108 and *crn* roots (supplementary table 1). We
416 found 19 genes to be up-, and 10 genes to be down-regulated in *crn* roots relative to wild-type
417 roots (logFC>1 or <-1, padj<0.05; Fig. 7A, supplementary table 7). Among the functionally
418 annotated genes down-regulated in *R. irregularis* colonizing *crn* roots relative to wild-type roots
419 (logFC<-1, padj<0.05), we identified multiple transcripts putatively involved in cellular signaling,
420 including two protein tyrosine kinases, a C2H2 zinc finger transcription factor, and one SAM-
421 domain containing protein, which mediate protein-protein interactions and have many roles,
422 including cellular signaling (Kim, 2003). This suggests that *R. irregularis* modulates signaling in
423 response to colonizing *crn* roots; however, because AM fungi are functionally not well
424 understood, we cannot predict which signaling pathways may be impacted.
425
426 Among the *R. irregularis* genes significantly up-regulated in *crn* roots relative to wild-type roots
427 (logFC>1, padj<0.05), we identified multiple transcripts that suggest fungal N metabolism might
428 be perturbed in *crn* (Fig. 7A). Differentially regulated genes associated with fungal N metabolism
429 include an argininosuccinate synthase (*ASS*), which is involved in the biosynthesis of arginine, a
430 critical component of N storage in AM fungi (Cruz *et al.*, 2007). In addition, among the
431 significantly up-regulated genes we found a transcript annotated as *NmrA (Nitrogen metabolic*
432 *regulation A)-like protein*, which in other fungi is part of a protein complex that functions in
433 transcriptional regulation of N metabolism based on N availability (Andrianopoulos *et al.*, 1998;
434 Stammers, 2001). Both *ASS* and *NmrA* have been predominantly detected in the extraradical

435 mycelium of AM fungi where N is taken up (Dumas-Gaudot *et al.*, 2004; Tian *et al.*, 2010). Other
436 known genes involved in *R. irregularis* N metabolism tended to be up-regulated in *crn* roots
437 relative to wildtypes (Fig. 7B), although the adjusted p-value did not fall below the stringent
438 significance criteria described above. This included the ammonium transporters *GintAMT1* and
439 *GintAMT3*, but not *GintAMT2*, two glutamine synthetases (*GS1, GS2*) and a N transporter (*NT*)
440 (Fellbaum *et al.*, 2012) (Fig. 7B).
441
442 Interestingly, a plasma membrane H^+-transporting ATPase HA1 with suggested roles in fungal P
443 sensing (Xie *et al.*, 2022) was also observed among the *R. irregulari*s genes significantly up-
444 regulated in *crn* roots (Fig. 7A). This observation prompted us to examine other transcripts
445 known to be involved in fungal in P homeostasis and transport (Kikuchi *et al.*, 2014, 2016; Xie *et*
446 *al.*, 2022). Although none of the known P homeostasis or transport genes were differentially
447 regulated in *crn* vs. R108 roots, some displayed trends toward increased expression in *crn*
448 relative to R108 (Fig. 7C). This included, among others, the Pi:H^+ symporter RiPT thought to be
449 involved in fungal P uptake from the environment (Harrison and van Buuren, 1995; Maldonado-
450 Mendoza *et al.*, 2001) and the Pi stress marker PHO2 (Austin and Mayer, 2020).
451
452 In addition, our *R. irregularis* transcriptome displays signs of increased chitin biosynthesis when
453 colonizing *crn* roots (Fig. 7A, supplementary table 7). Among the *R. irregularis* genes
454 significantly up-regulated in *crn* relative to R108 roots (logFC>1, padj<0.05), we identified a gene
455 encoding a UDP-N-acetylglucosamine diphosphorylase, which catalyzes the formation of
456 GlcNAc, and a chitin synthase, which catalyzes chitin formation from GlcNAc building blocks (Fig.
457 7A) (Chen *et al.*, 2022). Notably, GlcNAc are also building blocks of LCO and CO molecules
458 critical for pre-symbiotic communication with the host. Myc-LCO and CO production is
459 promoted by host strigolactones (Genre *et al.*, 2013); biosynthesis genes for these
460 phytohormones are induced in *crn* roots relative to wildtypes (Fig. 6), which could be linked to
461 the observed up-regulation of GlcNAc in *R. irregularis*. However, while fungal LCO and CO
462 molecules initiate CSSP signaling in the host upon recognition by plant LysM-type RLKs, they
463 also have a more general function in regulating fungal growth and development (Rush *et al.*,

464 2020). In addition, a member of the SGNH hydrolase/GDSL lipase family was up-regulated.
465 Although the specific function of this gene is unknown, SGNH hydrolases catalyze a variety of
466 carbon-modifying reactions (Anderson *et al.*, 2022), which may be related to fungal growth and
467 development within the host plant.
468
469 Together, our fungal transcriptome dataset suggests that *crn* roots results stimulate *R.*
470 *irregularis* N and P metabolism, growth and development. Notably, it is possible that some of
471 these changes are an indirect consequence of higher fungal colonization levels observed in the
472 mutant; however, the lack of differential regulation of *R. irregularis* housekeeping genes
473 between *crn* and wild-type roots (Supplementary table 8) suggests that the observed gene
474 expression differences are not solely caused by increased fungal biomass in *crn* roots. While
475 more research is required, our data supports the hypothesis that the *R. irregularis* differentially
476 responds to as-yet-unknown signals derived from *crn* and wild-type roots.
477
478 **Discussion**
479 CLV signaling has been reported to modulate various aspects of plant development and
480 responses to the environment (Bashyal *et al.*, 2023; Lindsay *et al.*, 2023). Here we describe *M.*
481 *truncatula CRN* as a central regulator of meristem branching and root interactions with AM
482 fungi.
483
484 Although legume mutants in the CLV signaling pathway have been well-studied in multiple plant
485 species in the context of symbiosis regulation, an effect on meristem development has only
486 been described in soybean and pea (Krusell *et al.*, 2011; Mirzaei *et al.*, 2017). Soybean encodes
487 two CLV1 copies, one of which controls symbiosis and the other controls meristem development
488 (Mirzaei *et al.*, 2017). Our work contributes to a better understanding of legume inflorescence
489 meristem patterning by revealing a role for *MtCRN* and *SUNN* in this process. Although the
490 molecular mechanisms remain to be determined, several hints in our data and that of others
491 point toward an intersection of auxin and CLV in *M. truncatula* meristem signaling: Auxin is an
492 important regulator of meristem identity, and *AtCRN* was found to act upstream of auxin to

493 control floral primordia outgrowth in Arabidopsis (Jones et al., 2021). The *M. truncatula* auxin
494 transport mutant *smooth leaf margin1* has pleiotropic developmental effects, including multiple
495 flowers per inflorescence that are reminiscent of the *crn* flower phenotype reported here (Zhou
496 et al, 2011), suggesting that *MtCRN* may control auxin-mediated outgrowth in *M. truncatula*
497 floral development similar to what was found in Arabidopsis (Jones et al., 2021). In addition,
498 previous studies reported that *SUNN* regulates shoot-to-root auxin transport to control N
499 response (Jin *et al.*, 2012) and that auxin signaling, among other hormonal pathways, is mis-
500 regulated in *sunn* (Karlo *et al.*, 2020, Preprint), further supporting the hypothesis that CLV
501 signaling may act upstream of auxin also in the context of *M. truncatula* meristem maintenance.
502 Like in Arabidopsis, legume meristem signaling may be controlled by multiple, functionally
503 redundant pathways and/or buffering. Consequently, phenotypes may only be apparent in
504 certain mutant alleles or growth conditions. Because these buffering mechanisms appear
505 distinct among plant species, this may explain why inflorescence meristem branching is
506 primarily affected in Medicago *crn* mutants, resembling the phenotype in other legumes (Krusell
507 *et al.*, 2011; Mirzaei *et al.*, 2017), but inflorescence meristem size is affected in maize and
508 Arabidopsis *crn* mutants (Rodriguez-Leal et al., 2019, Hazak and Hardtke, 2016, Je et al., 2016).
509
510 CLV signaling has been previously described to be critical for autoregulation of AM symbiosis
511 (AOM), but our knowledge on the molecular mechanisms remains limited. We previously
512 reported the up-regulation of three *MtCLE* genes in *R. irregularis*-inoculated roots, one of which
513 was functionally characterized as a member of the AOM pathway (*MtCLE53*) (Müller *et al.*,
514 2019; Karlo *et al.*, 2020, Preprint). *MtCLE53* requires *SUNN* to regulate AM symbiosis (Crook *et*
515 *al.*, 2016; Müller *et al.*, 2019; Karlo *et al.*, 2020, Preprint). Because MtCRN and SUNN can
516 interact and are required to perceive nodulation-associated CLE peptides during AON (Crook *et*
517 *al.*, 2016; Nowak *et al.*, 2019), we hypothesized that MtCRN may also be required for MtCLE53
518 signaling together with SUNN. However, the data presented here suggests that the negative
519 effect of *MtCLE53* overexpression on AM symbiosis is only partially dependent on *MtCRN*. One
520 possible explanation for our observation is that MtCLE53 can signal through MtCRN-SUNN but
521 also parallel, MtCRN-independent pathway(s). Such parallel pathways and compensation

522 mechanisms are common in CLAVATA signaling modules (Pallakies and Simon, 2014; Nimchuk,
523 2017; Je *et al.*, 2018; Rodriguez-Leal *et al.*, 2019; Selby and Jones, 2023). This also suggests that
524 additional, *MtCLE53*-independent pathways contribute to the elevated AM fungal root
525 colonization observed in *crn*. MtCRN can interact not only with CLV1 (SUNN) but also other
526 receptors, including MtCLV2 (Crook *et al.*, 2016); therefore it is possible that CRN is involved in
527 the signal transduction from multiple input signals. Multiple CLV signaling pathways also appear
528 to govern AM symbiosis in tomato (*Solanum lycopersicum*); for example, SlCLV2 was reported to
529 regulate AM symbiosis through two distinct local and systemic signaling pathways (Wang *et al.*,
530 2021; Wulf *et al.*, 2024). Previously published *MtCRN* promoter-reporter analyses revealed that
531 *MtCRN* is expressed in all root cell types with higher expression in the vascular tissue (Crook *et*
532 *al.*, 2016). *SUNN*, *MtCLE53*, and other symbiosis autoregulation regulators such as *MtRDN1* and
533 *MtDAR*, are also expressed in the vasculature (Schnabel *et al.*, 2012, 2024; Müller *et al.*, 2019;
534 Serrano *et al.*, 2024). Therefore, it is possible that a MtCLE53-SUNN-MtCRN autoregulatory
535 module regulates AM symbiosis through long-distance signaling in the vascular tissue, whereas
536 *MtCRN* expressed in other root cell types may have a distinct signaling function to regulate AM
537 symbiosis in concert with other partners.
538
539 Our transcriptomics experiment revealed that *M. truncatula crn* mutants display signatures of
540 abiotic stress, most notably nutrient starvation as suggested by a transcriptional up-regulation
541 of N, P and other nutrient transporters. It is possible that perpetually heightened nutrient
542 starvation signals promote AM symbiosis in *crn* independently of AOM. Nutrient-regulated CLE
543 peptides have been identified and CLV receptors have been implicated in various plant
544 responses to nutrient availability (including P and N) (Bashyal *et al.*, 2023); thus, it is tempting to
545 speculate that signaling of nutrient-induced CLE peptides may be perturbed in *crn*. Intriguingly,
546 *R. irregularis* also displays signs of disrupted N and P metabolism as indicated by an up-
547 regulation of *NmrA and ASS*. The proteins encoded by these genes are predicted to function in
548 the extracellular mycelium of AM fungi to mediate N utilization and incorporation into arginine
549 (Andrianopoulos *et al.*, 1998; Cruz *et al.*, 2007; Fellbaum *et al.*, 2012). Arginine plays a key role
550 in N translocation from the extra- to the intraradical mycelium in AM fungi (Cruz *et al.*, 2007;

551 Fellbaum *et al.*, 2012). In addition, *R. irregularis HA1* expression was increased when colonizing
552 *crn* roots; *RiHA1* was previously implicated in P signaling and uptake by the extraradical
553 mycelium, where it powers Pi:H^+ symporters to promote phosphate uptake (Ezawa and Saito,
554 2018; Xie *et al.*, 2022). Together with our host transcriptomics data, this finding suggests that
555 *crn* roots may represent a greater sink for N and P than wild-types and consequently stimulate N
556 and P uptake in the colonizing *R. irregularis* symbiont (Cruz *et al.*, 2007). Further research is
557 required to better understand the impact of host genotype and host CLV signaling on symbiont
558 metabolism.
559
560 In the plant, N and P starvation results in the upregulation of genes involved in the biosynthesis
561 of strigolactones, which in turn act as positive regulators of AM symbiosis (Akiyama *et al.*, 2005;
562 Yoneyama *et al.*, 2007; Liu *et al.*, 2011; Foo *et al.*, 2013, 2014; Marro *et al.*, 2022). Intriguingly,
563 our data reveal that many of these genes are upregulated in *crn* relative to wildtype controls,
564 which may be a direct consequence of the apparent perturbations in N and P signaling in *crn*.
565 Strigolactone biosynthesis is also the target of AOM, and the elevated expression of
566 strigolactone biosynthesis genes may also be caused by an at least partial disruption of AOM. In
567 either case, upregulation of genes involved in the symbiosis-promoting strigolactones in *crn* can
568 explain the elevated root colonization levels in the mutant. Together, our functional and
569 transcriptomic data suggests that MtCRN may act upstream of strigolactone biosynthesis
570 regulation in response to MtCLE53 and/or N and P signaling. Intriguingly, up-regulation of
571 strigolactone biosynthesis genes have not been observed in CLV1 mutants in *M. truncatula*
572 (*sunn*), pea (*nark*) or tomato (*fab*) (Foo *et al.*, 2014; Karlo *et al.*, 2020, Preprint; Wang *et al.*,
573 2021), suggesting that CRN (but not SUNN/FAB) may modulate cross-talk between N and P
574 homeostasis, MtCLE53-mediated autoregulation, and AM fungal root colonization.
575
576 Apart from genes involved in nutrient homeostasis and strigolactone biosynthesis, our
577 transcriptome analysis also suggests that *crn* roots display an upregulation of genes associated
578 with the CSSP. The CSSP is activated upon perception of diffusible LCO or CO signals derived
579 from AM fungi or rhizobia and is required for cellular entry of the microbial symbionts. Because

580 *crn* has previously been described as a regulator of nodulation symbiosis, an effect of *crn* on
581 CSSP gene expression may contribute not only to the hypermycorrhizal phenotype described
582 here, but also to the hypernodulation phenotype described previously (Crook *et al.*, 2016). It
583 was reported previously in rice that transcription of certain CSSP genes (including orthologs of
584 *MtVPY, DMI2, DMI3, IPD3*, which we found here to be regulated by *crn*) is regulated by the plant
585 phosphate starvation response (Das *et al.*, 2022). In addition, expression of LysM-type RLKs and
586 LysM receptor proteins as well as plant responses to LCO/CO perception depend on N and P
587 status of the plant and are greatly increased upon nutrient starvation (Li *et al.*, 2022). We
588 therefore hypothesize that the perturbed N and P signaling in *crn* promotes AM symbiosis by
589 increasing the expression of genes involved in early symbiosis signaling (strigolactone
590 biosynthesis genes, CSSP genes, LysM-RLKs), which facilitates colonization by AM fungi upon
591 contact. It has been established that nutrient starvation determines the outcome of plant-
592 microbe interactions by fine-tuning plant immune responses, potentially in order to facilitate
593 symbiotic interactions (Paries and Gutjahr, 2023). Consistent with this model, our dataset
594 suggests attenuated oxidative stress in *crn* relative to wildtypes; oxidative stress is a hallmark of
595 responses to abiotic factors but also plant immunity. However, we also detected up-regulation
596 of plant defense genes, suggesting *crn* displays additional signatures of enhanced response to
597 biotic stress. Complex biotic stress responses have been described before for *crn*: For example,
598 *A. thaliana crn* mutants display increased resistance to *Heterodera schachtii* cyst nematodes as
599 well as certain bacterial and oomycete pathogens (*Ralstonia solanacearum* and
600 *Hyaloperonospora arabidopsidis*, respectively), while being more susceptible to *Botrytis*
601 necrotrophic fungi or *Pseudomonas syringae* bacterial infection (Replogle *et al.*, 2011;
602 Hanemian *et al.*, 2016). Together with our data, this suggests that coordination or cross-talk of
603 multiple combined abiotic and/or biotic stress responses, rather than overall stress signaling,
604 may be impaired in *crn*.
605
606 In summary, our findings suggest that *MtCRN* plays multiple, likely independent, roles in plant
607 development, nutrient homeostasis, and plant interactions with the environment. Based on
608 data from other plant species, where different combinations of CLV1-type receptors, CLV2, and

609 CRN are responsible for the perception of diverse CLE signals in a context- and cell-type-specific
610 manner (Whitewoods, 2021), we propose that *MtCRN* acts downstream of diverse CLE peptides
611 in the context of meristem development, nutrient homeostasis, and plant-microbe interactions.
612 More research is needed to identify additional context-dependent CLE signals and receptors
613 that provide specificity to the various signaling pathways *MtCRN* is involved in.
614
615 **Materials and methods**
616
617 **Plant materials and growth conditions**
618 Homozygous *M. truncatula crn* (NF3436) and *sunn-5* (NF2262) mutants, both in R108
619 background, were a gift from Dr. Julia Frugoli (Clemson University, SC, USA) and were previously
620 described (Crook *et al.*, 2016; Nowak *et al.*, 2019; Thomas and Frugoli, 2024).
621 For AM inoculation experiments, seeds were extracted from seed pods and scarified using
622 sandpaper or by incubating the seeds in concentrated sulfuric acid for 7 minutes. Seeds were
623 washed 5 times in autoclaved distilled H2O and surface-sterilized with 10% Bleach for 7
624 minutes. Seeds were rinsed again 5 times in autoclaved distilled H2O and incubated at 4°C for
625 48 hours. Imbibed seeds were germinated on germination paper (Anchor paper) for 3-5 days at
626 room temperature before transplanting into substrate. Plants were grown as previously
627 described (Chaulagain *et al.*, 2023*a*). In brief, germinated seedlings were transplanted into SC10
628 cone-tainers (Steuwe and Sons) filled with washed and autoclaved substrate mix consisting of
629 play sand and fine vermiculite (1:1 ratio). For inoculated samples, 250 *Rhizophagus irregularis*
630 DAOM197198 spores (Premier Tech, Canada) were placed onto a sand layer 5 cm below the
631 surface of the substrate in each cone-tainer. For mock-inoculated samples, an equal amount of
632 distilled water was added onto the sand layer. Plants were grown in a growth chamber under a
633 16 hour light (24°C)/8 hour dark (22°C) regime at 40% relative humidity. For standard
634 experiments, all cones were fertilized twice per week with 20 ml half-strength Hoagland's
635 fertilizer supplied with 20µM potassium phosphate. Unless otherwise noted, all plants were
636 harvested 5-6 weeks after inoculation. To enrich for *R. irregularis* colonization, we sampled 5

637 cm-long root sections centered around the inoculated region. For the transcriptomics
638 experiment, whole root systems were harvested.
639
640 **Transient root transformation**
641 Transient root transformations of *M. truncatula* R108 and *crn* plants with *35S:GUS* and
642 *35S:MtCLE53* constructs were performed as described previously (Boisson-Dernier *et al.*, 2001;
643 Müller *et al.*, 2019). Chimeric plants were inoculated with *R. irregularis* as described above and
644 harvested 6.5 weeks after planting into cone-tainers.
645
646 **Root system phenotyping**
647 Seeds were extracted from seed pods and sterilized as described above. Seeds were then
648 distributed on the bottom of a glass petri dish using water surface tension (Floss *et al.*, 2013).
649 Glass petri plates were placed upside down in a 28°C incubator and seedlings were allowed to
650 germinate overnight. With this method, we were able to obtain seedlings with straight roots.
651 Seedlings were then transferred to 12x12 cm square petri dishes filled with modified Fahraeus
652 (F) medium supplied with 4 g/L Gelzan CM agar (Sigma-Aldrich) (Floss *et al.*, 2013). Plates were
653 placed at a 45° angle in a growth chamber under a 16 hour light (24°C)/8 hour dark (22°C)
654 regime. The bottom 2/3 of the plates was wrapped in aluminum foil to protect the roots from
655 light. Pictures of seedlings were taken every 3 days for 12 days starting with the day of transfer
656 to agar plates (day 0). Root system parameters (primary root length, lateral root length, lateral
657 root number, lateral root density) were analyzed using the SmartRoot package in Fiji (Lobet *et*
658 *al.*, 2011; Schindelin *et al.*, 2012) for each timepoint.
659
660 **AM fungus staining, microscopy, and quantification of AM fungal colonization**
661 WGA-Alexafluor488 staining was performed by incubating the roots in 20% KOH for 3-4 days at
662 65°C. Roots were rinsed 3-5 times with distilled water and incubated in 1xPBS overnight.
663 Cleared and washed roots were stained with 0.2 mg/ml WGA-Alexafluor488 (Invitrogen) in
664 1xPBS for at least 6 hours. Stained roots were visualized using a Leica Thunder Imager or a Leica
665 M205 FA stereomicroscope. Root length colonization was assessed using the grid-line method

666 (McGonigle *et al.*, 1990). Arbuscule and vesicle density was quantified as previously described
667 (Müller *et al.*, 2020; Chaulagain *et al.*, 2023*a*). In brief, a minimum of 5 z-stacks each of
668 randomly selected colonized root sections from at least 3 independent root systems were
669 imaged that encompassed all arbuscules in that area. Roots were positioned so that the
670 hyphopodium was at the center of the image to ensure infections were at a comparable
671 developmental stage. Imaged arbuscules were counted using the Fiji Image Analysis Package
672 (Schindelin *et al.*, 2012), which was also used to accurately measure the imaged root length.
673 Arbuscule density (arbuscules/mm) was calculated by dividing the number of arbuscules by the
674 root length. Confocal images were obtained using a Leica SP5 confocal microscope.
675
676 **Transcriptomics**
677 For each genotype (*crn* and R108), 6-week-old mock- (n=4 per genotype) and *R. irregularis*-
678 colonized root systems (n=3 per genotype) were harvested as described above. WGA-
679 Alexafluor488 staining was performed on a subset of the samples to confirm colonization. RNA
680 was extracted from the remaining samples as previously described (Javot *et al.*, 2011). Library
681 preparation and transcriptome sequencing was performed by Novogene Co, Ltd. Samples were
682 enriched for mRNA using poly(A) capture. Paired-end sequencing (PE150) was performed on the
683 Illumina Novaseq X platform. Sequencing raw data is deposited in the NCBI Sequence Read
684 Archive (SRA) (BioProject PRJNA1140176). Filtered reads were mapped against the *M.*
685 *truncatula* Mt4.0v1 genome (downloaded from Phytozome 13) and *R. irregularis* DAOM
686 RhiirDAOM197198 v2.0 (downloaded from the JGI Mycocosm database) genome using HiSAT2
687 (Tang *et al.*, 2014; Kim *et al.*, 2019; Yildirir *et al.*, 2022). Normalized read counts were used to
688 calculate differential gene expression with DESeq2 (Love *et al.*, 2014). For each pairwise
689 comparison, log2-transformed fold changes were obtained for each mapped gene. Differential
690 gene expression was considered significant if the p-value adjusted for multiple comparisons
691 using Benjamini-Hochberg method (padj) was below 0.05. Heatmaps were constructed using
692 FPKM-normalized read counts; rows were clustered using Pearson correlation, columns using
693 Spearman correlation. To identify gene groups with similar expression patterns across samples,
694 hierarchical clustering was performed on FPKM-normalized read counts averaged for each

genotype/treatment. The number of clusters (k=6) was determined using the sum of squared error method. GO term analysis for biological process was performed on https://geneontology.org/; visualization of the obtained GO term enrichment results was performed in R.

Scanning electron microscopy

For inflorescence phenotyping, plants were grown in 6-inch azalea pots in soil (Promix) under a 16 hour light/8 hour dark regime at 20-22°C and watered with distilled water as needed. Axils from 8-week-old plants were dissected with 30 gauge insulin syringe needles to reveal inflorescence meristems under a stereoscope. Meristems and the surrounding tissue were mounted on stubs using double-sided tape and imaged in a Jeol JCM-7000 benchtop scanning electron microscope (SEM) with the following conditions: high vacuum, 15 kV, high probe current, analysis mode. Meristems from SEM images were categorized based on (Benlloch *et al.*, 2003) and measured using Fiji.

Statistical analyses

Statistical significance between two experimental groups was assessed using two-sided Student's t-test. In graphs, statistical significances between two groups are represented as follows: ***$p<0.001$; **$p<0.01$; *$p<0.05$. Statistical significance between multiple experimental groups was calculated with ANOVA, followed by Tukey's HSD test for multiple comparisons. Pairwise comparisons were considered statistically significant if $p<0.05$. Significant differences are denoted with different letters. The % reduction of root length colonization shown in Fig. 3 was calculated separately for each genotype by the following formula: ((sample $RLC_{35S:CLE53}$ – average $RLC_{35S:GUS}$)/average $RLC_{35S:GUS}$)*100. The % reduction values for each genotype were then compared to each other using student's t-test. See paragraphs 'transcriptomics' for additional details on the statistics used to analyze RNA sequencing data. Graphs show data from individual experiments. All experiments were repeated at least twice with similar results.

Acknowledgements

We thank Julia Frugoli (Clemson University, SC) for kindly gifting us the *crn* and *sunn-5* mutant lines. We also thank Dr. Yerisf Torres Ascurra for helpful discussions and critically reading the manuscript.

Author contributions

L.M.M. conceived the project. J.O., E.X.L, M.K., S.B., H.E., C.K.G. and L.M.M. performed all experiments except for the inflorescence meristem analyses, which were performed by P.L.L. L.M.M. and D.J. acquired funding for the project. L.M.M. wrote the manuscript with input from all co-authors.

Conflict of interest

None to declare.

Funding

This work was partially funded by USDA-NIFA award 2022-67013-42820 to L.M.M. and an American Society of Plant Biologists (ASPB) Summer Undergraduate Research Fellowships (SURF) fellowship to E.X.L. P.L.L. and D.J. were funded by USDA-NIFA award 2020-67013-30909.

Data availability

Raw data from the transcriptome sequencing has been deposited on the NCBI SRA database (Bioproject ID: PRJNA1140176).

753 **Figure legends**

754

755 **Figure 1: *M. truncatula CRN* impacts inflorescence development.** A) Close-up of R108 wild-type
756 flower. 100% of inflorescences produced a solitary flower in our growth conditions. B) Dissected
757 wild-type flower. Std, standard petal; fused keel and 2 wing petals; c+s, carpel and stamen. C)
758 Close-up of inflorescence produced by *crn*. Note the additional undeveloped bud (arrowhead).
759 In our growth conditions, 91% of *crn* produced two flowers per inflorescence, the remaining 9%
760 produced solitary flowers similar to the one shown in (A). D) Dissected *crn* flower. Flower organ
761 number and morphology appeared similar to the R108 wildtype shown in (B). (A-D) Scale bars:
762 0.5 mm. E) Scanning electron microscopy images of R108 and *crn* inflorescence meristems. In
763 *M. truncatula*, the primary inflorescence meristem (I_1) produces a secondary inflorescence
764 meristem (I_2) and leaf primordium (L). The secondary meristem will in turn produce a floral
765 meristem (F), which will differentiate floral organ primordia. Top panels show stage five floral
766 meristems, in which all floral organ primordia have been established. Floral organ primordia size
767 and number are unaltered in *crn*, but there is a second stage 5 floral meristem, indicated with
768 an asterisk. The bottom panel shows a range of floral meristem stages in R108 and *crn*. In *crn,*
769 two I_2 meristems are present at the same time, indicated by an asterisk. C, carpel primordium,
770 k, keel petal, s_{ab}, abaxial sepal, st_p, non-fused vexillary stamen, st_s, antesepal stamen, v_x,
771 vexillum, Br, bract. Scale bar: 100 µm. F) Width of R108 and *crn* meristems in different floral
772 meristem stages. No effect of the *crn* mutation was observed on meristem width in any
773 developmental stage assessed. I_2, secondary inflorescence meristem, F, floral meristem, in
774 which sepal primordia begin to form, stage 4, in which common primordia that will form
775 stamens and petals are formed, stage 5, in which all floral organ primordia have been
776 established. G) Number of stamen and petal floral organ primordia in stage 5 meristems. N.s.,
777 no significant difference between R108 and *crn* (Student's t-test).

778

779 **Figure 2: *M. truncatula crn* mutants display elevated levels of colonization by the AM fungus**
780 ***R. irregularis*.** A) *crn* mutants diplay higher levels of overall root length colonization relative to
781 R108 wild-type controls. B) *crn* mutants show higher arbuscule density (number of arbuscules

per mm colonized root length) relative to R108 wild-type controls. C) Vesicle density (vesicles per mm colonized root length) does not differ between R108 and *crn*. D) Representative image of an *R. irregularis*-colonized R108 wildtype root. *R. irregularis* was stained with WGA-Alexafluor488 (green). Dashed line: outline of the root. E) Representative image of an *R. irregularis* (green) colonized root section in *crn*. Dashed line: outline of the root. A-C) Bar plots show averages, error bars the standard deviation, points represent individual measurements (i.e., n=4 individual root systems per genotype in A) and n=19 (R108) and n=25 (*crn*) imaged root sections in B) and C), derived from the same root systems as shown in A). Graphs display data from one experiment; this experiment was repeated twice with similar results. ** $p<0.01$ (t-test). Scale bar in D), E): 100 µm.

Figure 3: AM fungal root length colonization of *crn* mutants partially depend on *MtCLE53*. Graph depicts average root length colonization (%) of R108 and *crn* plants transformed with the *35S::GUS (GUS)* or the *35S::MtCLE53 (CLE53)* construct. *MtCLE53* over-expression reduces *R. irregularis* root colonization in R108 and *crn*; however, this suppressive effect is stronger in R108 than in *crn*. For each genotype, the % of colonization reduction upon *MtCLE53* over-expression is shown. The bar graph shows average values, error bars denote standard deviation. Black dots indicate individual datapoints (biological replicates; n=3-5 replicates per sample). This graph displays data from one experiment; the experiment was repeated twice with similar results. Different letters denote significant differences ($p<0.05$) after ANOVA ($p=2.12*10^{-5}$) followed by Tukey's HSD test for pairwise comparisons.

Figure 4: Hierarchical cluster analysis of differentially expressed genes in *R. irregularis*-colonized and mock-inoculated *crn* and R108 wild-type roots. A) 1655 genes that are differentially expressed between *R. irregularis*-colonized *crn* and R108 wild-type roots (log2 fold-change >1 or <-1, padj<0.05) were selected for cluster analysis to identify gene groups with similar expression patterns. Genes were clustered using Pearson correlation. Heatmap shows averages of n=4 root samples each for *crn* and R108 mock-inoculated, and n=3 samples each for *crn* and R108 *R. irregularis*-inoculated (*R.i.*). Gene lists for each cluster can be found in table S2.

811 Line graphs display normalized relative expression changes across samples for each individual
812 gene in a cluster (grey) and average changes in color. B) Biological functions GO terms enriched
813 in cluster 1, C) Biological functions GO terms enriched in cluster 2, D) Biological functions GO
814 terms enriched in cluster 6. Note: Cluster 4 has one significantly enriched GO term "plant-type
815 secondary cell wall biogenesis", which is not shown in this figure. Supplementary tables 2 and 3
816 contains a list of genes for each cluster and the associated GO terms, respectively. DXP, 1-deoxy-
817 d-xylulose 5-phosphate. FDR, false discovery rate.
818
819 **Figure 5: Differential regulation of N and P homeostasis genes in *crn* mutants.** A) Heatmap for
820 genes annotated as *NITRATE TRANSPORTER (NRT), NITRATE AND PEPTIDE TRANSPORTER FAMILY*
821 *(NPF), NITRATE ASSIMILATION RELATED (NAR), AMMONIUM TRANSPORTER (AMT),* and *NITRATE*
822 *REDUCTASE (NR)* with putative roles in *M. truncatula* N metabolism. B) Venn diagram showing
823 the number of putative N homeostasis genes responding to AM symbiosis, *crn*, or both
824 (padj<0.05). C) Venn diagram showing the number of putative P homeostasis genes responding
825 to AM symbiosis, *crn*, or both (padj<0.05). D) Heatmap for genes annotated as *PHOSPHATE*
826 *TRANSPORTER (PT), PHOSPHATE1 (PHO), PHOSPHATE STARVATION RESPONSE (PHR* and *PHR-*
827 *LIKE, PHRL),* or *SYG1/PHO81/XPR1 family (SPX)* with putative roles in P homeostasis and
828 transport. A and D) Heatmaps show averages of n=4 root samples each for *crn* and R108 mock-
829 inoculated, and n=3 samples each for *crn* and R108 *R. irregularis*-inoculated (*R.i.*). AM-regulated
830 genes are highlighted in grey, genes differentially regulated in *crn* vs. R108 with no effect of
831 colonization status in light green. Genes responsive to AM and *crn* are highlighted in dark green.
832 B and C) 'AM-regulated' is defined as genes with differential regulation (padj<0.05) between
833 *R.irregularis*-colonized and mock-inoculated R108 and/or *crn* roots, respectively. '*crn*-regulated'
834 is defined as genes with differential regulation (padj<0.05) in mock-inoculated *crn* relative to
835 mock-inoculated R108 roots. Transcript data used to produce these heatmaps can be found in
836 Supplementary table 4.
837
838 **Figure 6: Differential regulation of AM symbiosis regulators in *crn* mutants.** A) Heatmaps for
839 known genes involved in pre-symbiotic signaling, the common symbiosis signaling pathway

840 (CSSP) shared between AM and nodulation symbiosis, arbuscule accommodation, and arbuscule
841 degradation. B) Venn diagram showing the number of AM regulatory genes from panel A)
842 responding to AM symbiosis, *crn*, or both. C) Venn diagram showing the number of LysM-RLK or
843 LysM receptor protein-encoding genes (LYK, LYR, LYM) responding to AM symbiosis, *crn*, or both.
844 D) Heatmap for LysM-RLK genes in mock- and *R. irregularis*-inoculated wildtype (R108) and *crn*
845 roots. A and D) Heatmaps show averages of n=4 root samples each for *crn* and R108 mock-
846 inoculated, and n=3 samples each for *crn* and R108 *R. irregularis*-inoculated (*R.i.*). AM-regulated
847 genes are highlighted in grey, genes differentially regulated in *crn* vs. R108 with no effect of
848 colonization status in light green. Genes responsive to AM and *crn* are highlighted in dark green.
849 B and C) 'AM-regulated' is defined as genes with differential regulation (padj<0.05) between *R.*
850 *irregularis*-colonized and mock-inoculated R108 and/or *crn* roots, respectively. '*crn*-regulated' is
851 defined as genes with differential regulation (padj<0.05) in mock-inoculated *crn* relative to
852 mock-inoculated R108 roots. Transcript data used to produce these heatmaps can be found in
853 supplementary tables 5 and 6.
854
855 **Figure 7: Host genotype-dependent regulation of *R. irregularis* gene expression.** A)
856 Differentially expressed *R. irregularis* genes (log2 fold change >1 or <-1, padj<0.05) in *crn* and
857 R108 roots. B) Heatmap of genes involved in fungal N metabolism. C) Heatmap of genes
858 involved in fungal P metabolism. Significance: ***adjusted p-value (padj)<0.05, **padj<0.01,
859 *padj<0.05; if no symbol is shown, fungal gene expression does not significantly differ between
860 host genotypes. Transcript data used to produce these heatmaps can be found in
861 supplementary table 7. Data for the same Argininosuccinate synthase (*ASS*) gene is shown in
862 panels A) and B); data for the same H^+-transporting ATPase (*HA1*) gene is shown in panels A)
863 and C).
864
865
866
867
868

References

Abbott LK, Robson AD, de Boer G. 1984. THE EFFECT OF PHOSPHORUS ON THE FORMATION OF HYPHAE IN SOIL BY THEVESICULAR-ARBUSCULAR MYCORRHIZAL FUNGUS, *GLOMUS FASCICULATUM*. The new phytologist **97**, 437–446.

Akiyama K, Matsuzaki K-I, Hayashi H. 2005. Plant sesquiterpenes induce hyphal branching in arbuscular mycorrhizal fungi. Nature **435**, 824–827.

Anderson AC, Stangherlin S, Pimentel KN, Weadge JT, Clarke AJ. 2022. The SGNH hydrolase family: a template for carbohydrate diversity. Glycobiology **32**, 826.

Andrianopoulos A, Kourambas S, Sharp JA, Davis MA, Hynes MJ. 1998. Characterization of the Aspergillus nidulans nmrA gene involved in nitrogen metabolite repression. Journal of bacteriology **180**, 1973–1977.

Austin S, Mayer A. 2020. Phosphate homeostasis − A vital metabolic equilibrium maintained through the INPHORS signaling pathway. Frontiers in microbiology **11**.

Bashyal S, Gautam CK, Müller LM. 2023. CLAVATA signaling in plant–environment interactions. Plant physiology doi: 10.1093/plphys/kiad591.

Benlloch R, Navarro C, Beltrán J, Cañas LA. 2003. Floral development of the model legume Medicago truncatula: ontogeny studies as a tool to better characterize homeotic mutations. Sexual plant reproduction **15**, 231–241.

Bleckmann A, Weidtkamp-Peters S, Seidel CAM, Simon R. 2009. Stem cell signaling in Arabidopsis requires CRN to localize CLV2 to the plasma membrane. Plant physiology **152**, 166–176.

Boisson-Dernier A, Chabaud M, Garcia F, Bécard G, Rosenberg C, Barker DG. 2001. Agrobacterium rhizogenes-transformed roots of Medicago truncatula for the study of nitrogen-fixing and endomycorrhizal symbiotic associations. Molecular plant-microbe interactions: MPMI **14**, 695–700.

Buendia L, Girardin A, Wang T, Cottret L, Lefebvre B. 2018. LysM Receptor-Like Kinase and LysM Receptor-Like Protein Families: An Update on Phylogeny and Functional Characterization. Frontiers in plant science **9**, 539.

Chaulagain D, Schnabel E, Crook A, Bashyal S, Müller LM, Frugoli J. 2023*a*. A mutation in mediator subunit MED16A suppresses nodulation and increases arbuscule density in Medicago truncatula. Journal of plant growth regulation doi: 10.1007/s00344-023-10993-2.

Chaulagain D, Schnabel E, Lin EX, Garcia RR, Noorai RE, Müller LM, Frugoli JA. 2023*b*. *TML1*AND*TML2*SYNERGISTICALLY REGULATE NODULATION BUT NOT ARBUSCULAR MYCORRHIZA IN*MEDICAGO TRUNCATULA*. bioRxiv.

Chen W, Cao P, Liu Y, *et al.* 2022. Structural basis for directional chitin biosynthesis. Nature **610**, 402–408.

Chen Y, Miao Y, Huang L, Li J, Sun H, Zhao Y, Yang J, Zhou W. 2014. Antioxidant activities of saponins extracted from Radix Trichosanthis: an in vivo and in vitro evaluation. BMC complementary and alternative medicine **14**, 86.

Clark SE, Williams RW, Meyerowitz EM. 1997. The CLAVATA1 gene encodes a putative receptor kinase that controls shoot and floral meristem size in Arabidopsis. Cell **89**, 575–585.

Crook AD, Schnabel EL, Frugoli JA. 2016. The systemic nodule number regulation kinase SUNN in Medicago truncatula interacts with MtCLV2 and MtCRN. The Plant journal: for cell and molecular biology **88**, 108–119.

Cruz C, Egsgaard H, Trujillo C, Ambus P, Requena N, Martins-Loução MA, Jakobsen I. 2007. Enzymatic evidence for the key role of arginine in nitrogen translocation by arbuscular mycorrhizal fungi. Plant physiology **144**, 782–792.

Das D, Paries M, Hobecker K, Gigl M, Dawid C, Lam H-M, Zhang J, Chen M, Gutjahr C. 2022. PHOSPHATE STARVATION RESPONSE transcription factors enable arbuscular mycorrhiza symbiosis. Nature communications **13**, 1–12.

Dumas-Gaudot E, Valot B, Bestel-Corre G, Recorbet G, St-Arnaud M, Fontaine B, Dieu M, Raes M, Saravanan RS, Gianinazzi S. 2004. Proteomics as a way to identify extra-radicular fungal proteins from Glomus intraradicesâ RiT-DNA carrot root mycorrhizas. FEMS microbiology ecology **48**, 401–411.

Ezawa T, Saito K. 2018. How do arbuscular mycorrhizal fungi handle phosphate? New insight into fine-tuning of phosphate metabolism. The new phytologist **220**, 1116–1121.

Fellbaum CR, Gachomo EW, Beesetty Y, Choudhari S, Strahan GD, Pfeffer PE, Kiers ET, Bücking H. 2012. Carbon availability triggers fungal nitrogen uptake and transport in arbuscular mycorrhizal symbiosis. Proceedings of the National Academy of Sciences of the United States of America **109**, 2666–2671.

Fester T, Hause G. 2005. Accumulation of reactive oxygen species in arbuscular mycorrhizal roots. Mycorrhiza **15**, 373–379.

Floss DS, Schmitz AM, Starker CG, Gantt JS, Harrison MJ. 2013. Gene Silencing in Medicago truncatula Roots Using RNAi. Methods in molecular biology (Clifton, N.J.). Legume Genomics. Totowa, NJ: Humana Press, 163–177.

Foo E, Ferguson BJ, Reid JB. 2014. The potential roles of strigolactones and brassinosteroids in the autoregulation of nodulation pathway. Annals of botany **113**, 1037–1045.

Foo E, Yoneyama K, Hugill CJ, Quittenden LJ, Reid JB. 2013. Strigolactones and the regulation of pea symbioses in response to nitrate and phosphate deficiency. Molecular plant **6**, 76–87.

Fujimatsu T, Endo K, Yazaki K, Sugiyama A. 2020. Secretion dynamics of soyasaponins in soybean roots and effects to modify the bacterial composition. Plant direct **4**.

Genre A, Chabaud M, Balzergue C, *et al.* 2013. Short-chain chitin oligomers from arbuscular mycorrhizal fungi trigger nuclear Ca2+ spiking in Medicago truncatula roots and their production is enhanced by strigolactone. The New phytologist **198**, 190–202.

Gullner G, Komives T, Király L, Schröder P. 2018. Glutathione S-Transferase Enzymes in Plant-Pathogen Interactions. Frontiers in plant science **9**.

Guo Y, Han L, Hymes M, Denver R, Clark SE. 2010. CLAVATA2 forms a distinct CLE-binding receptor complex regulating Arabidopsis stem cell specification. The Plant journal: for cell and molecular biology **63**, 889–900.

Hanemian M, Barlet X, Sorin C, *et al.* 2016. Arabidopsis CLAVATA1 and CLAVATA2 receptors contribute to Ralstonia solanacearum pathogenicity through a miR169-dependent pathway. The new phytologist **211**, 502–515.

Harrison MJ, van Buuren ML. 1995. A phosphate transporter from the mycorrhizal fungus Glomus versiforme. Nature **378**, 626–629.

Hazak O, Brandt B, Cattaneo P, Santiago J, Rodriguez-Villalon A, Hothorn M, Hardtke CS. 2017. Perception of root-active CLE peptides requires CORYNE function in the phloem vasculature. EMBO reports **18**, 1367–1381.

Hazak O, Hardtke CS. 2016. CLAVATA 1-type receptors in plant development. Journal of experimental botany **67**, 4827–4833.

He J, Zhao H, Cheng Z, Ke Y, Liu J, Ma H. 2019. Evolution analysis of the fasciclin-like arabinogalactan proteins in plants shows variable fasciclin-AGP domain constitutions. International journal of molecular sciences **20**, 1945.

Huang H, Ullah F, Zhou D-X, Yi M, Zhao Y. 2019. Mechanisms of ROS regulation of plant development and stress responses. Frontiers in plant science **10**.

Javot H, Penmetsa RV, Breuillin F, Bhattarai KK, Noar RD, Gomez SK, Zhang Q, Cook DR, Harrison MJ. 2011. Medicago truncatula mtpt4 mutants reveal a role for nitrogen in the regulation of arbuscule degeneration in arbuscular mycorrhizal symbiosis. The Plant journal: for cell and molecular biology **68**, 954–965.

Je BI, Xu F, Wu Q, Liu L, Meeley R, Gallagher JP, Corcilius L, Payne RJ, Bartlett ME, Jackson D. 2018. The CLAVATA receptor FASCIATED EAR2 responds to distinct CLE peptides by signaling through two downstream effectors. eLife **7**, e35673.

Jin J, Watt M, Mathesius U. 2012. The autoregulation gene SUNN mediates changes in root organ formation in response to nitrogen through alteration of shoot-to-root auxin transport. Plant physiology **159**, 489–500.

Jones DS, John A, VanDerMolen KR, Nimchuk ZL. 2021. CLAVATA signaling ensures reproductive development in plants across thermal environments. Current biology: CB **31**, 220-227.e5.

Karlo M, Boschiero C, Landerslev KG, Blanco GS, Wen J, Mysore KS, Dai X, Zhao PX, de Bang TC. 2020. The CLE53–SUNN genetic pathway negatively regulates arbuscular mycorrhiza root colonization in Medicago truncatula.

Kikuchi Y, Hijikata N, Ohtomo R, Handa Y, Kawaguchi M, Saito K, Masuta C, Ezawa T. 2016. Aquaporin-mediated long-distance polyphosphate translocation directed towards the host in arbuscular mycorrhizal symbiosis: application of virus-induced gene silencing. The new phytologist **211**, 1202–1208.

Kikuchi Y, Hijikata N, Yokoyama K, Ohtomo R, Handa Y, Kawaguchi M, Saito K, Ezawa T. 2014. Polyphosphate accumulation is driven by transcriptome alterations that lead to near-synchronous and near-equivalent uptake of inorganic cations in an arbuscular mycorrhizal fungus. The new phytologist **204**, 638–649.

Kim C. 2003. SAM domains: uniform structure, diversity of function. Trends in biochemical sciences **28**, 625–628.

Kim D, Paggi JM, Park C, Bennett C, Salzberg SL. 2019. Graph-based genome alignment and genotyping with HISAT2 and HISAT-genotype. Nature biotechnology **37**, 907–915.

Krusell L, Sato N, Fukuhara I, *et al.* 2011. The *Clavata2* genes of pea and *Lotus japonicus* affect autoregulation of nodulation. The Plant journal: for cell and molecular biology **65**, 861–871.

Li X-R, Sun J, Albinsky D, *et al.* 2022. Nutrient regulation of lipochitooligosaccharide recognition in plants via NSP1 and NSP2. Nature communications **13**, 1–15.

Limpens E, Franken C, Smit P, Willemse J, Bisseling T, Geurts R. 2003. LysM Domain Receptor Kinases Regulating Rhizobial Nod Factor-Induced Infection. Science **302**, 630–633.

Lindsay PL, Ivanov S, Pumplin N, Zhang X, Harrison MJ. 2022. Distinct ankyrin repeat subdomains control VAPYRIN locations and intracellular accommodation functions during arbuscular mycorrhizal symbiosis. Nature communications **13**, 5228.

Lindsay P, Swentowsky KW, Jackson D. 2023. Cultivating potential: Harnessing plant stem cells for agricultural crop improvement. Molecular plant doi: 10.1016/j.molp.2023.12.014.

Liu W, Kohlen W, Lillo A, *et al.* 2011. Strigolactone biosynthesis in Medicago truncatula and rice requires the symbiotic GRAS-type transcription factors NSP1 and NSP2. The Plant cell **23**, 3853–3865.

Lobet G, Pagès L, Draye X. 2011. A novel image-analysis toolbox enabling quantitative analysis of root system architecture. Plant physiology **157**, 29–39.

Love MI, Huber W, Anders S. 2014. Moderated estimation of fold change and dispersion for RNA-seq data with DESeq2. Genome biology **15**, 550.

MacLean AM, Bravo A, Harrison MJ. 2017. Plant Signaling and Metabolic Pathways Enabling Arbuscular Mycorrhizal Symbiosis. The Plant cell **29**, 2319–2335.

Maldonado-Mendoza IE, Dewbre GR, Harrison MJ. 2001. A phosphate transporter gene from the extra-radical mycelium of an arbuscular mycorrhizal fungus *Glomus intraradices* is regulated in response to phosphate in the environment. Molecular plant-microbe interactions: MPMI **14**, 1140–1148.

Marone D, Russo M, Laidò G, De Leonardis A, Mastrangelo A. 2013. Plant nucleotide binding site–leucine-rich repeat (NBS-LRR) genes: Active guardians in host defense responses. International journal of molecular sciences **14**, 7302–7326.

Marro N, Lidoy J, Chico MÁ, Rial C, García J, Varela RM, Macías FA, Pozo MJ, Janoušková M, López-Ráez JA. 2022. Strigolactones: New players in the nitrogen–phosphorus signalling interplay. Plant, cell & environment **45**, 512–527.

McGonigle PT, Miller MH, Evans DG, Fairchild GL, Swan JA. 1990. A new method which gives an objective measure of colonization of roots by vesicular-arbuscular mycorrhizal fungi. The New phytologist **150**, 495–501.

Mirzaei S, Batley J, El-Mellouki T, Liu S, Meksem K, Ferguson BJ, Gresshoff PM. 2017. Neodiversification of homeologous CLAVATA1-like receptor kinase genes in soybean leads to distinct developmental outcomes. Scientific reports **7**.

Morandi D, Sagan M, Prado-Vivant E, Duc G. 2000. Influence of genes determining supernodulation on root colonization by the mycorrhizal fungus Glomus mosseae in Pisum sativum and Medicago truncatula mutants. Mycorrhiza **10**, 37–42.

Mortier V, Den Herder G, Whitford R, Van de Velde W, Rombauts S, D'Haeseleer K, Holsters M, Goormachtig S. 2010. CLE peptides control Medicago truncatula nodulation locally and systemically. Plant physiology **153**, 222–237.

Mugford ST, Osbourn A. 2012. Saponin synthesis and function. Isoprenoid Synthesis in Plants and Microorganisms. New York, NY: Springer New York, 405–424.

Müller R, Bleckmann A, Simon R. 2008. The receptor kinase CORYNE of Arabidopsis transmits the stem cell-limiting signal CLAVATA3 independently of CLAVATA1. The plant cell **20**, 934–946.

Müller LM, Campos-Soriano L, Lévesque-Tremblay V, Bravo A, Daniels DA, Pathak S, Park H-J, Harrison MJ. 2020. Constitutive Overexpression of RAM1 Leads to an Increase in Arbuscule Density in Brachypodium distachyon. Plant physiology **184**, 1263.

Müller LM, Flokova K, Schnabel E, Sun X, Fei Z, Frugoli J, Bouwmeester HJ, Harrison MJ. 2019. A CLE–SUNN module regulates strigolactone content and fungal colonization in arbuscular mycorrhiza. Nature plants **5**, 933–939.

Nimchuk ZL. 2017. CLAVATA1 controls distinct signaling outputs that buffer shoot stem cell proliferation through a two-step transcriptional compensation loop. PLoS genetics **13**, e1006681.

Nouri E, Breuillin-Sessoms F, Feller U, Reinhardt D. 2014. Phosphorus and nitrogen regulate arbuscular mycorrhizal symbiosis in petunia hybrida. PloS one **9**, e90841.

Nowak S, Schnabel E, Frugoli J. 2019. The Medicago truncatula CLAVATA3-LIKE CLE12/13 signaling peptides regulate nodule number depending on the CORYNE but not the COMPACT ROOT ARCHITECTURE2 receptor. Plant signaling & behavior **14**, 1598730.

Oldroyd GED. 2013. Speak, friend, and enter: signalling systems that promote beneficial symbiotic associations in plants. Nature reviews. Microbiology **11**, 252–263.

Pallakies H, Simon R. 2014. The CLE40 and CRN/CLV2 signaling pathways antagonistically control root meristem growth in Arabidopsis. Molecular plant **7**, 1619–1636.

Paries M, Gutjahr C. 2023. The good, the bad, and the phosphate: regulation of beneficial and detrimental plant–microbe interactions by the plant phosphate status. The new phytologist **239**, 29–46.

Passardi F, Cosio C, Penel C, Dunand C. 2005. Peroxidases have more functions than a Swiss army knife. Plant cell reports **24**, 255–265.

Replogle A, Wang J, Bleckmann A, Hussey RS, Baum TJ, Sawa S, Davis EL, Wang X, Simon R, Mitchum MG. 2011. Nematode CLE signaling in Arabidopsis requires CLAVATA2 and CORYNE. The Plant journal: for cell and molecular biology **65**, 430–440.

Rodriguez-Leal D, Xu C, Kwon C-T, *et al.* 2019. Evolution of buffering in a genetic circuit controlling plant stem cell proliferation. Nature genetics **51**, 786–792.

Roy S, Müller LM. 2022. A rulebook for peptide control of legume-microbe endosymbioses. Trends in plant science **27**, 870–889.

Rush TA, Puech-Pagès V, Bascaules A, *et al.* 2020. Lipo-chitooligosaccharides as regulatory signals of fungal growth and development. Nature communications **11**.

Schindelin J, Arganda-Carreras I, Frise E, *et al.* 2012. Fiji: an open-source platform for biological-image analysis. Nature methods **9**, 676–682.

Schnabel E, Bashyal S, Corbett C, Kassaw T, Nowak S, Rosales-García RA, Noorai RE, Müller LM, Frugoli J. 2024. The Defective in Autoregulation (DAR) gene of Medicago truncatula encodes a protein involved in regulating nodulation and arbuscular mycorrhiza. BMC plant biology **24**, 766.

Schnabel E, Journet E-P, de Carvalho-Niebel F, Duc G, Frugoli J. 2005. The Medicago truncatula SUNN gene encodes a CLV1-like leucine-rich repeat receptor kinase that regulates nodule number and root length. Plant molecular biology **58**, 809–822.

Schnabel E, Karve A, Kassaw T, Mukherjee A, Zhou X, Hall T, Frugoli J. 2012. The*M. truncatula SUNN*gene is expressed in vascular tissue, similarly to*RDN1*, consistent with the role of these nodulation regulation genes in long distance signaling. Plant signaling & behavior **7**, 4–6.

Selby R, Jones DS. 2023. Complex peptide hormone signaling in plant stem cells. Current opinion in plant biology **75**, 102442.

Serrano K, Bezrutczyk M, Goudeau D, Dao T, O'Malley R, Malmstrom RR, Visel A, Scheller HV, Cole B. 2024. Spatial co-transcriptomics reveals discrete stages of the arbuscular mycorrhizal symbiosis. Nature plants **10**, 673–688.

Smit P, Limpens E, Geurts R, Fedorova E, Dolgikh E, Gough C, Bisseling T. 2007. Medicago LYK3, an entry receptor in rhizobial nodulation factor signaling. Plant physiology **145**, 183–191.

Smith SE, Reid D. 2008. *Mycorrhizal Symbiosis*. Academic Press.

Somssich M, Bleckmann A, Simon R. 2016*a*. Shared and distinct functions of the pseudokinase CORYNE (CRN) in shoot and root stem cell maintenance of Arabidopsis. Journal of experimental botany **67**, 4901–4915.

Somssich M, Je BI, Simon R, Jackson D. 2016*b*. CLAVATA-WUSCHEL signaling in the shoot meristem. Development **143**, 3238–3248.

Stammers DK. 2001. The structure of the negative transcriptional regulator NmrA reveals a structural superfamily which includes the short-chain dehydrogenase/reductases. The EMBO journal **20**, 6619–6626.

Tang H, Krishnakumar V, Bidwell S, *et al.* 2014. An improved genome release (version Mt4.0) for the model legume Medicago truncatula. BMC genomics **15**, 312.

Thomas J, Frugoli J. 2024. Mutation of BAM2 rescues the sunn hypernodulation phenotype in Medicago truncatula, suggesting that a signaling pathway like CLV1/BAM in Arabidopsis affects nodule number. Frontiers in plant science **14**.

Tian C, Kasiborski B, Koul R, Lammers PJ, Bücking H, Shachar-Hill Y. 2010. Regulation of the nitrogen transfer pathway in the arbuscular mycorrhizal symbiosis: Gene characterization and the coordination of expression with nitrogen flux. Plant physiology **153**, 1175–1187.

Tsuno Y, Fujimatsu T, Endo K, Sugiyama A, Yazaki K. 2018. Soyasaponins: A New Class of Root Exudates in Soybean (Glycine max). Plant & cell physiology **59**, 366–375.

Vicente J, Cascón T, Vicedo B, García-Agustín P, Hamberg M, Castresana C. 2012. Role of 9-lipoxygenase and α-dioxygenase oxylipin pathways as modulators of local and systemic defense. Molecular plant **5**, 914–928.

Wang C, Reid JB, Foo E. 2018. The Art of Self-Control - Autoregulation of Plant-Microbe Symbioses. Frontiers in plant science **9**, 988.

Wang C, Velandia K, Kwon C-T, Wulf KE, Nichols DS, Reid JB, Foo E. 2021. The role of CLAVATA signalling in the negative regulation of mycorrhizal colonization and nitrogen response of tomato. Journal of experimental botany **72**, 1702–1713.

Whitewoods CD. 2021. Evolution of CLE peptide signalling. Seminars in cell & developmental biology **109**, 12–19.

Wojtaszek P. 1997. Oxidative burst: an early plant response to pathogen infection. The Biochemical journal **322**, 681–692.

Wulf K, Sun J, Wang C, *et al.* 2024. The role of CLE peptides in the suppression of mycorrhizal colonization of tomato. Plant & cell physiology **65**, 107–119.

Xie X, Lai W, Che X, Wang S, Ren Y, Hu W, Chen H, Tang M. 2022. A SPX domain-containing phosphate transporter from *Rhizophagus irregularis* handles phosphate homeostasis at symbiotic interface of arbuscular mycorrhizas. The new phytologist **234**, 650–671.

Xie Z, Nolan TM, Jiang H, Yin Y. 2019. AP2/ERF transcription factor regulatory networks in hormone and abiotic stress responses in Arabidopsis. Frontiers in plant science **10**.

Yildirir G, Sperschneider J, Malar C M, Chen ECH, Iwasaki W, Cornell C, Corradi N. 2022. Long reads and Hi-C sequencing illuminate the two-compartment genome of the model arbuscular mycorrhizal symbiont *Rhizophagus irregularis*. The new phytologist **233**, 1097–1107.

Yoneyama K, Xie X, Kim HI, Kisugi T, Nomura T, Sekimoto H, Yokota T, Yoneyama K. 2012. How do nitrogen and phosphorus deficiencies affect strigolactone production and exudation? Planta **235**, 1197–1207.

Yoneyama K, Xie X, Kusumoto D, Sekimoto H, Sugimoto Y, Takeuchi Y, Yoneyama K. 2007. Nitrogen deficiency as well as phosphorus deficiency in sorghum promotes the production and exudation of 5-deoxystrigol, the host recognition signal for arbuscular mycorrhizal fungi and root parasites. Planta **227**, 125–132.

Zhang J, Sun J, Chiu CH, *et al.* 2024. A receptor required for chitin perception facilitates arbuscular mycorrhizal associations and distinguishes root symbiosis from immunity. Current biology: CB **34**, 1705-1717.e6.

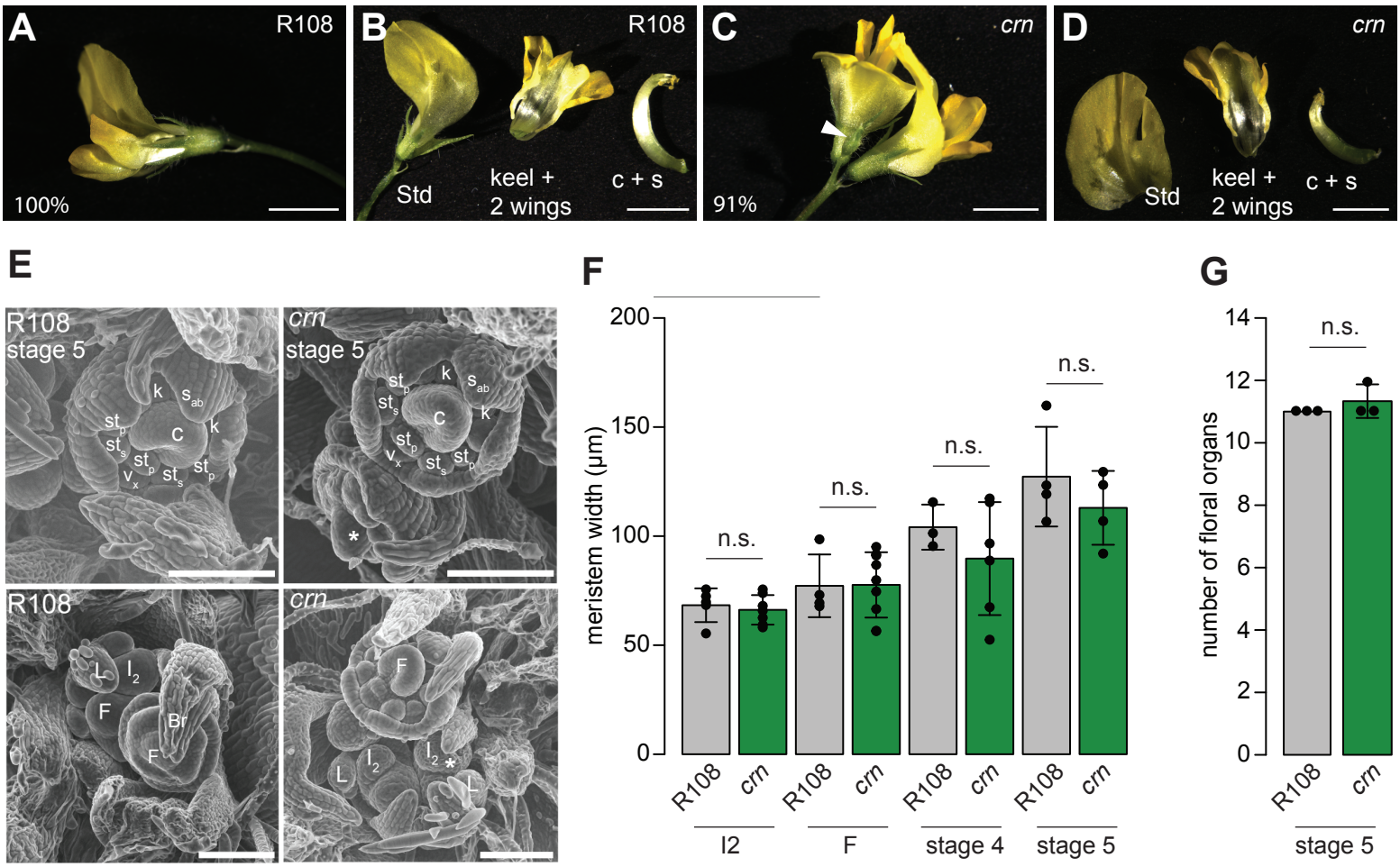

Figure 1: *M. truncatula CRN* impacts inflorescence development. A) Close-up of R108 wild-type flower. 100% of inflorescences produced a solitary flower in our growth conditions. B) Dissected wild-type flower. Std, standard petal; fused keel and 2 wing petals; c+s, carpel and stamen. C) Close-up of inflorescence produced by *crn*. Note the additional undeveloped bud (arrowhead). In our growth conditions, 91% of *crn* produced two flowers per inflorescence, the remaining 9% produced solitary flowers similar to the one shown in (A). D) Dissected *crn* flower. Flower organ number and morphology appeared similar to the R108 wildtype shown in (B). (A-D) Scale bars: 0.5 mm. E) Scanning electron microscopy images of R108 and *crn* inflorescence meristems. In *M. truncatula*, the primary inflorescence meristem (I1) produces a secondary inflorescence meristem (I2) and leaf primordium (L). The secondary meristem will in turn produce a floral meristem (F), which will differentiate floral organ primordia. Top panels show stage five floral meristems, in which all floral organ primordia have been established. Floral organ primordia size and number are unaltered in *crn*, but there is a second stage 5 floral meristem, indicated with an asterisk. The bottom panel shows a range of floral meristem stages in R108 and *crn*. In *crn*, two I2 meristems are present at the same time, indicated by an asterisk. C, carpel primordium, k, keel petal, sab, abaxial sepal, stp, non-fused vexillary stamen, sts, antesepal stamen, vx, vexillum, Br, bract. Scale bar: 100 µm. F) Width of R108 and *crn* meristems in different floral meristem stages. No effect of the *crn* mutation was observed on meristem width in any developmental stage assessed. I2, secondary inflorescence meristem, F, floral meristem, in which sepal primordia begin to form, stage 4, in which common primordia that will form stamens and petals are formed, stage 5, in which all floral organ primordia have been established. G) Number of stamen and petal floral organ primordia in stage 5 meristems. N.s., no significant difference between R108 and *crn* (Student's t-test).

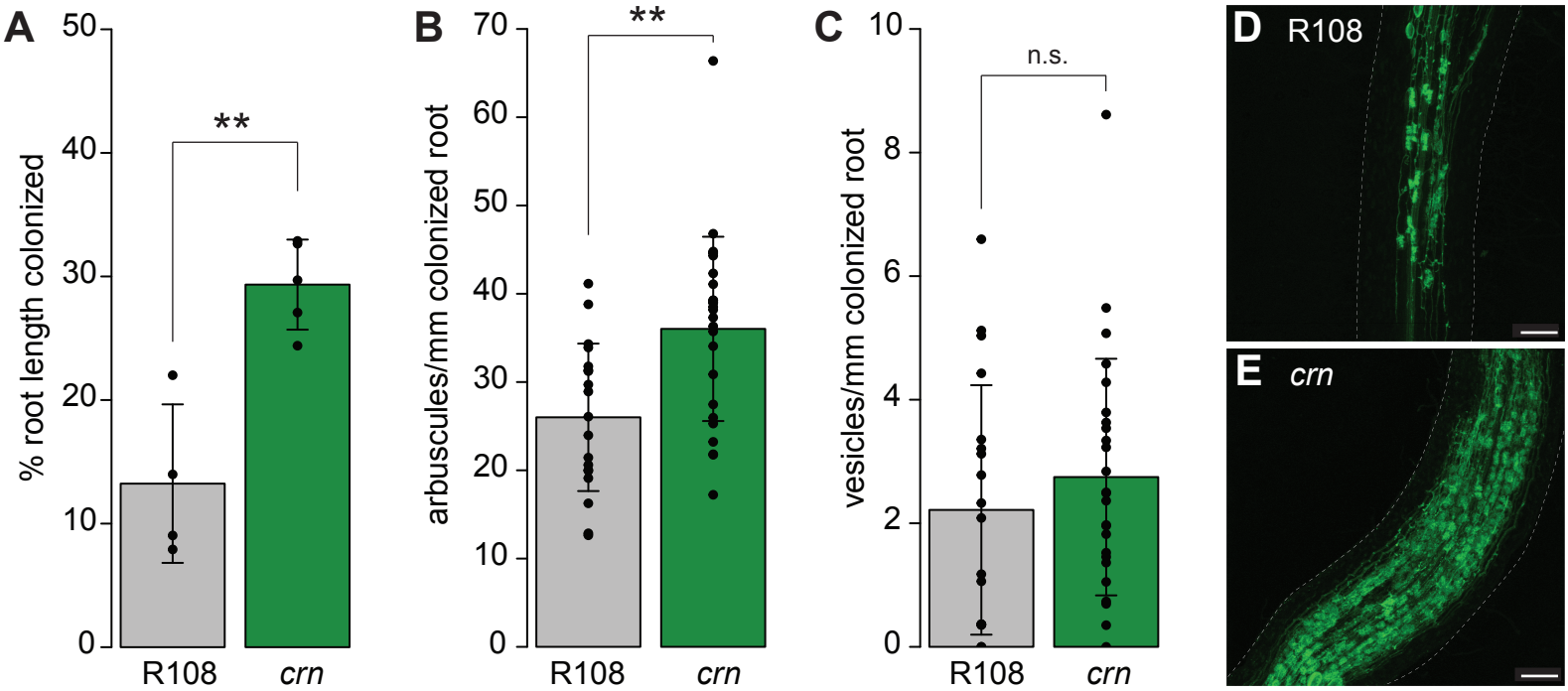

Figure 2: *M. truncatula crn* mutants display elevated levels of colonization by the AM fungus *R. irregularis*. A) *crn* mutants diplay higher levels of overall root length colonization relative to R108 wild-type controls. B) *crn* mutants show higher arbuscule density (number of arbuscules per mm colonized root length) relative to R108 wild-type controls. C) Vesicle density (vesicles per mm colonized root length) does not differ between R108 and *crn*. D) Representative image of an *R. irregularis*-colonized R108 wildtype root. R. irregularis was stained with WGA-Alexafluor488 (green). Dashed line: outline of the root. E) Representative image of an *R. irregularis* (green) colonized root section in crn. Dashed line: outline of the root. A-C) Bar plots show averages, error bars the standard deviation, points represent individual measurements (i.e., n=4 individual root systems per genotype in A) and n=19 (R108) and n=25 (*crn*) imaged root sections in B) and C), derived from the same root systems as shown in A). Graphs display data from one experiment; this experiment was repeated twice with similar results. ** $p<0.01$ (t-test). Scale bar in D), E): 100 µm.

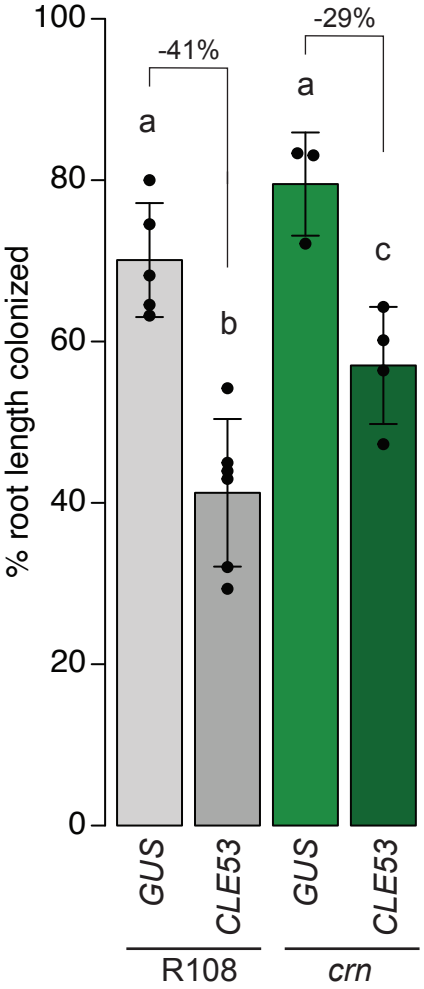

Figure 3: AM fungal root length colonization of *crn* mutants partially depend on *MtCLE53*. Graph depicts average root length colonization (%) of R108 and *crn* plants transformed with the *35S::GUS (GUS)* or the *35S::MtCLE53 (CLE53)* construct. *MtCLE53* over-expression reduces *R. irregularis* root colonization in R108 and *crn*; however, this suppressive effect is stronger in R108 than in *crn*. For each genotype, the % of colonization reduction upon *MtCLE53* over-expression is shown. The bar graph shows average values, error bars denote standard deviation. Black dots indicate individual datapoints (biological replicates; n=3-5 replicates per sample). This graph displays data from one experiment; the experiment was repeated twice with similar results. Different letters denote significant differences ($p<0.05$) after ANOVA ($p=2.12*10-5$) followed by Tukey's HSD test for pairwise comparisons.

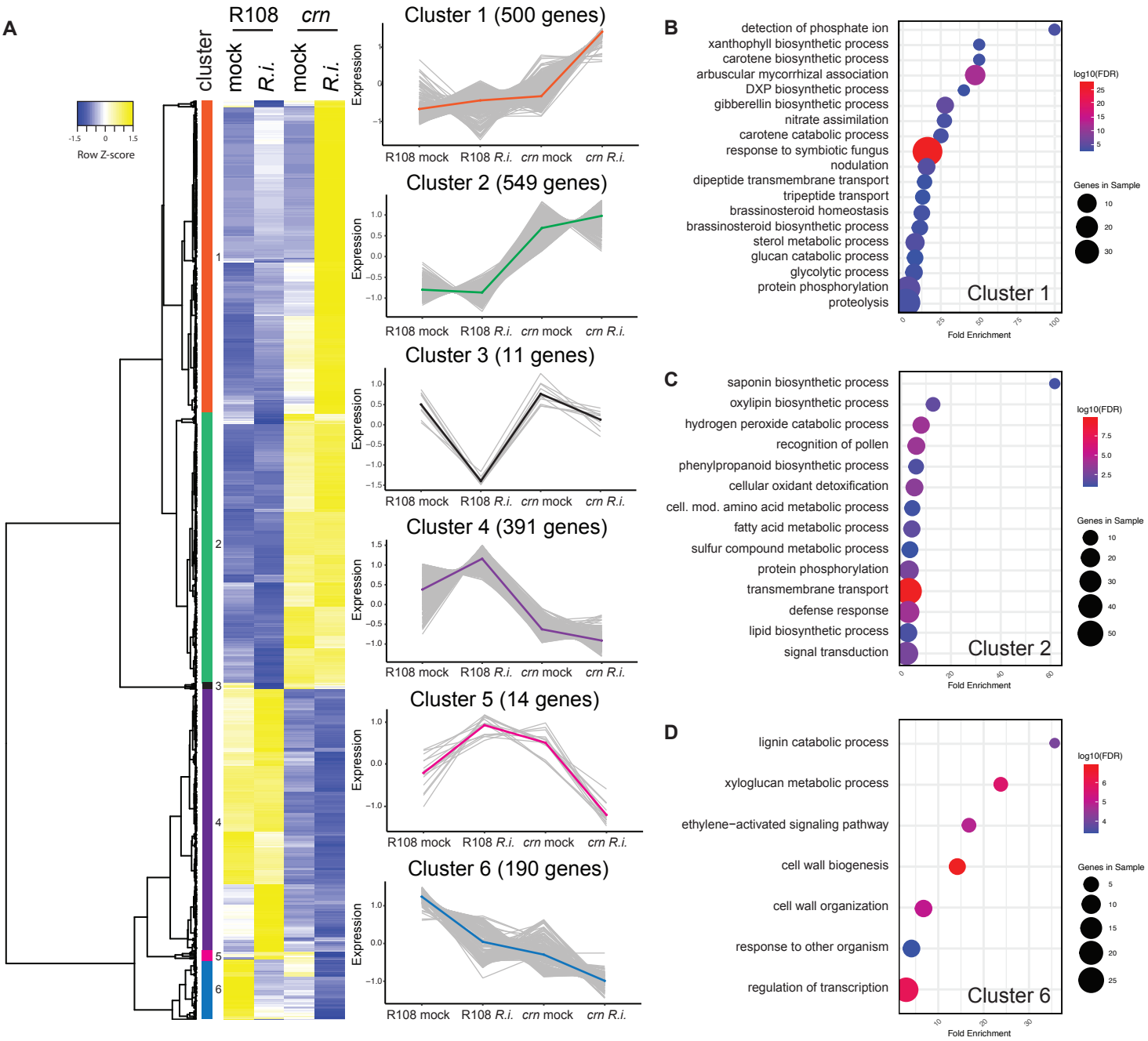

Figure 4: Hierarchical cluster analysis of differentially expressed genes in *R. irregularis*-colonized and mock-inoculated *crn* and R108 wild-type roots. A) 1655 genes that are differentially expressed between *R. irregularis*-colonized crn and R108 wild-type roots (log2 fold-change >1 or <-1, padj<0.05) were selected for cluster analysis to identify gene groups with similar expression patterns. Genes were clustered using Pearson correlation. Heatmap shows averages of n=4 root samples each for *crn* and R108 mock-inoculated, and n=3 samples each for crn and R108 *R. irregularis*-inoculated (R.i.). Gene lists for each cluster can be found in table S2. Line graphs display normalized relative expression changes across samples for each individual gene in a cluster (grey) and average changes in color. B) Biological functions GO terms enriched in cluster 1, C) Biological functions GO terms enriched in cluster 2, D) Biological functions GO terms enriched in cluster 6. Note: Cluster 4 has one significantly enriched GO term “plant-type secondary cell wall biogenesis”, which is not shown in this figure. Supplementary tables 2 and 3 contains a list of genes for each cluster and the associated GO terms, respectively. DXP, 1-deoxy-d-xylulose 5-phosphate. FDR, false discovery rate.

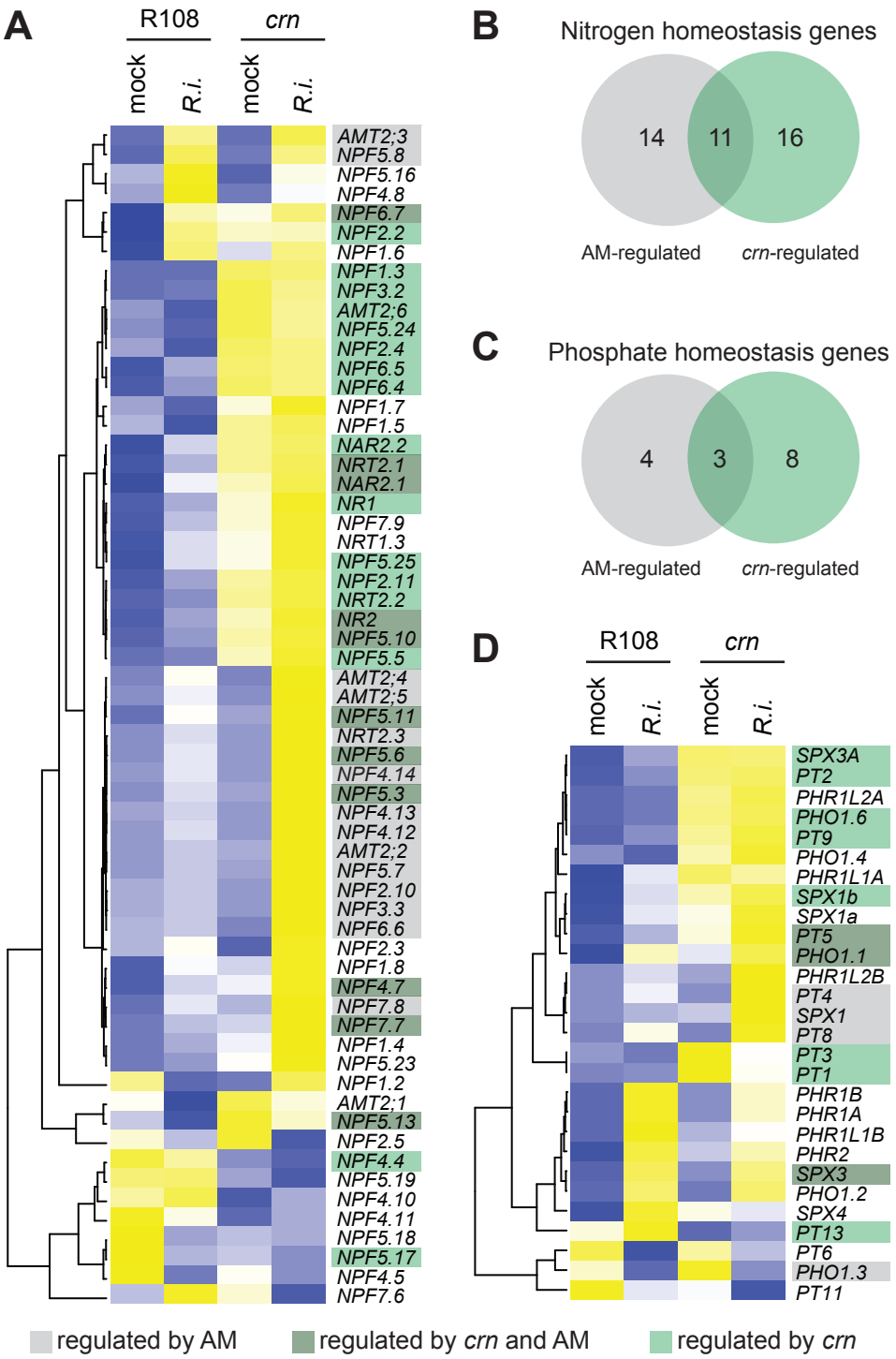

Figure 5: Differential regulation of N and P homeostasis genes in crn mutants. A) Heatmap for genes annotated as *NITRATE TRANSPORTER (NRT), NITRATE AND PEPTIDE TRANSPORTER FAMILY (NPF), NITRATE ASSIMILATION RELATED (NAR), AMMONIUM TRANSPORTER (AMT),* and *NITRATE REDUCTASE (NR)* with putative roles in *M. truncatula* N metabolism. B) Venn diagram showing the number of putative N homeostasis genes responding to AM symbiosis, *crn*, or both (padj<0.05). C) Venn diagram showing the number of putative P homeostasis genes responding to AM symbiosis, *crn*, or both (padj<0.05). D) Heatmap for genes annotated as *PHOSPHATE TRANSPORTER (PT), PHOSPHATE1 (PHO), PHOSPHATE STARVATION RESPONSE (PHR and PHR-LIKE, PHRL),* or *SYG1/PHO81/XPR1 family (SPX)* with putative roles in P homeostasis and transport. A and D) Heatmaps show averages of n=4 root samples each for *crn* and R108 mock-inoculated, and n=3 samples each for crn and R108 *R. irregularis*-inoculated (R.i.). AM-regulated genes are highlighted in grey, genes differentially regulated in *crn* vs. R108 with no effect of colonization status in light green. Genes responsive to AM and *crn* are highlighted in dark green. B and C) 'AM-regulated' is defined as genes with differential regulation (padj<0.05) between *R. irregularis*-colonized and mock-inoculated R108 and/or *crn* roots, respectively. '*crn*-regulated' is defined as genes with differential regulation (padj<0.05) in mock-inoculated *crn* relative to mock-inoculated R108 roots. Transcript data used to produce these heatmaps can be found in Supplementary table 4.

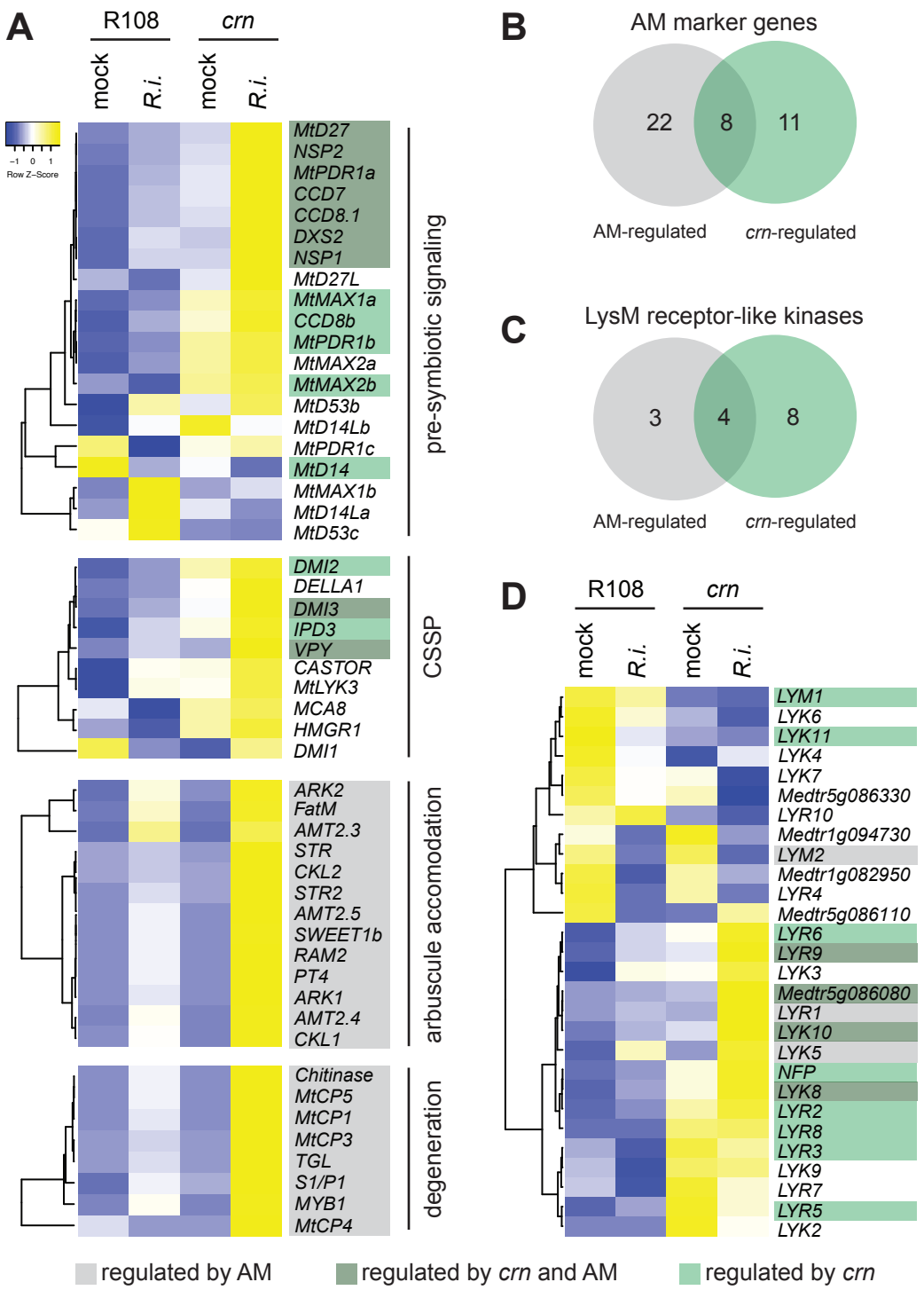

Figure 6: Differential regulation of AM symbiosis regulators in *crn* mutants. A) Heatmaps for known genes involved in pre-symbiotic signaling, the common symbiosis signaling pathway (CSSP) shared between AM and nodulation symbiosis, arbuscule accommodation, and arbuscule degradation. B) Venn diagram showing the number of AM regulatory genes from panel A) responding to AM symbiosis, *crn*, or both. C) Venn diagram showing the number of LysM-RLK or LysM receptor protein-encoding genes (LYK, LYR, LYM) responding to AM symbiosis, *crn*, or both. D) Heatmap for LysM-RLK genes in mock- and *R. irregularis*-inoculated wildtype (R108) and crn roots. A and D) Heatmaps show averages of n=4 root samples each for *crn* and R108 mock-inoculated, and n=3 samples each for *crn* and R108 *R. irregularis*-inoculated (R.i.). AM-regulated genes are highlighted in grey, genes differentially regulated in *crn* vs. R108 with no effect of colonization status in light green. Genes responsive to AM and *crn* are highlighted in dark green. B and C) 'AM-regulated' is defined as genes with differential regulation (padj<0.05) between *R. irregularis*-colonized and mock-inoculated R108 and/or *crn* roots, respectively. '*crn*-regulated' is defined as genes with differential regulation (padj<0.05) in mock-inoculated *crn* relative to mock-inoculated R108 roots. Transcript data used to produce these heatmaps can be found in supplementary tables 5 and 6.

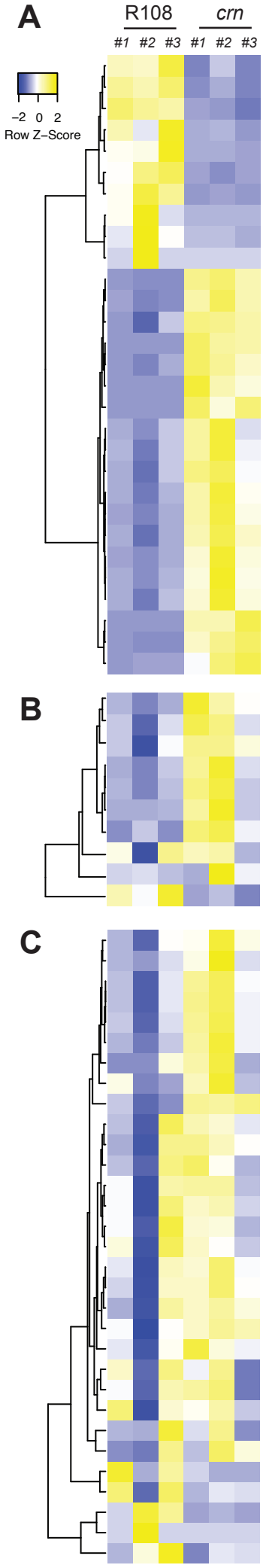

Transcript ID	log2FC *crn* vs. R108	Annotation/Predicted function
RhiirDAOM197198_2|9844	-2.14*	*SAM domain protein*
RhiirDAOM197198_2|13293	-2.74*	*C2H2 zinc finger trancription factor*
RhiirDAOM197198_2|16818	-3.22*	*Protein tyrosin kinase*
RhiirDAOM197198_2|17307	-1.51*	*Hypothetical protein*
RhiirDAOM197198_2|2319	-1.94*	*Protein tyrosin kinase*
RhiirDAOM197198_2|23682	-2.60*	*Reverse transcriptase*
RhiirDAOM197198_2|14123	-5.98*	*N/A*
RhiirDAOM197198_2|7238	-4.53*	*N/A*
RhiirDAOM197198_2|16170	-4.56*	*Hypothetical protein*
RhiirDAOM197198_2|2249	-21.77***	*N/A*
RhiirDAOM197198_2|19584	6.28**	*HMG-box transcription factor*
RhiirDAOM197198_2|11721	3.92*	*Hypothetical protein*
RhiirDAOM197198_2|18715	1.47*	*Chitin synthase*
RhiirDAOM197198_2|17083	6.61*	*Protein tyrosin kinase*
RhiirDAOM197198_2|14848	3.98**	*SGNH hydrolase*
RhiirDAOM197198_2|9973	6.34*	*N/A*
RhiirDAOM197198_2|17489	6.61*	*BTB/POZ domain protein*
RhiirDAOM197198_2|20306	2.05*	*Argininosuccinate synthase (ASS)*
RhiirDAOM197198_2|19511	1.59*	*Plasma membrane H+-transporting ATPase (HA1)*
RhiirDAOM197198_2|20706	1.43*	*UDP-N-acetylglucosamine pyrophosphorylase*
RhiirDAOM197198_2|1007	2.03**	*Hypothetical protein*
RhiirDAOM197198_2|6666	1.99***	*NmrA-like family transcriptional regulator*
RhiirDAOM197198_2|2903	1.95**	*Hypothetical protein*
RhiirDAOM197198_2|5108	3.78**	*Hypothetical protein*
RhiirDAOM197198_2|15466	1.74*	*Hypothetical protein*
RhiirDAOM197198_2|3941	1.64*	*Hypothetical protein*
RhiirDAOM197198_2|23251	6.57*	*Hypothetical protein*
RhiirDAOM197198_2|22853	6.05**	*S-adenosyl-L-methionine-dependent methyltransferase*
RhiirDAOM197198_2|6347	3.08*	*Hypothetical protein*
RhiirDAOM197198_2|5990	3.17	*Glutamine synthetase 1 (GS1)*
RhiirDAOM197198_2|9451	1.87	*Ammonium transporter 1 (AMT1)*
RhiirDAOM197198_2|15678	1.05	*Ammonium transporter 3 (AMT3)*
RhiirDAOM197198_2|20306	2.05*	*Argininosuccinate synthase (ASS)*
RhiirDAOM197198_2|19029	1.55	*Glutamine synthetase 2 (GS2)*
RhiirDAOM197198_2|19267	0.52	*Urease (URE)*
RhiirDAOM197198_2|6647	1.03	*Nitrate transporter (NT)*
RhiirDAOM197198_2|16597	0.21	*Ammonium transporter 2 (AMT2)*
RhiirDAOM197198_2|6495	0.24	*Argininosuccinate lyase (AL)*
RhiirDAOM197198_2|4355	-1.37	*Ornithine decarboxylase (ODC)*
RhiirDAOM197198_2|23514	1.33	*Endopolyphosphatase 1-2 (PPN1-2)*
RhiirDAOM197198_2|18246	1.79	*Pi:H+ symporter (RiPT)*
RhiirDAOM197198_2|20391	0.98	*Vacuolar H+-ATPase subunit (Vma10)*
RhiirDAOM197198_2|15404	1.70	*Acid phosphatase 5-4 (ACP5-4)*
RhiirDAOM197198_2|8727	1.55	*Pi:H+ symporter (RiPT1)*
RhiirDAOM197198_2|19511	1.59*	*Plasma membrane H+-transporting ATPase (HA1)*
RhiirDAOM197198_2|20738	NA	*Cyclin-dependent kinase (PHO85p)*
RhiirDAOM197198_2|4944	1.62	*Pi:H+ symporter (RiPT3)*
RhiirDAOM197198_2|2233	2.65	*Homeobox transcription factor (PHO2)*
RhiirDAOM197198_2|8874	0.52	*Glycerophosphoinositol glycerophosphodiesterase (Gde1p)*
RhiirDAOM197198_2|25249	0.84	*Vacuolar transporter chaperone 2 (VTC2)*
RhiirDAOM197198_2|6499	0.56	*Vacuolar transporter chaperone 4 (VTC4)*
RhiirDAOM197198_2|19120	0.80	*Exopolyphosphatase (PPX1)*
RhiirDAOM197198_2|24749	0.63	*Inositol pyrophosphate synthase (VIP1)*
RhiirDAOM197198_2|4688	0.25	*Aquaporin 3 (AQP3)*
RhiirDAOM197198_2|4273	0.21	*Na+ /dicarboxylate/Pi cotransporter (RiPT7)*
RhiirDAOM197198_2|12076	0.73	*Acid phosphatase 5-1 (ACP5.1)*
RhiirDAOM197198_2|18673	1.19	*Na+ /Pi symporter (RiPT6)*
RhiirDAOM197198_2|15520	0.27	*Basic-helix-loop-helix transcription factor (PHO4)*
RhiirDAOM197198_2|2178	0.93	*CDK inhibitor (PHO81p)*
RhiirDAOM197198_2|9081	0.87	*Plasma membrane H+-transporting ATPase (HA2)*
RhiirDAOM197198_2|24792	-0.14	*Endopolyphosphatase 1-1 (PPN1-1)*
RhiirDAOM197198_2|2694	0.66	*EXS family phosphate transporter (SYG1)*
RhiirDAOM197198_2|20810	0.36	*Alkaline phosphatase 2 (ALP2)*
RhiirDAOM197198_2|9564	-0.22	*Vacuolar transporter chaperone 1 (VTC1)*
RhiirDAOM197198_2|15696	0.18	*Na+ /Pi symporter (RiPT5)*
RhiirDAOM197198_2|19120	0.80	*Endopolyphosphatase 1 (PPN1)*
RhiirDAOM197198_2|6199	-0.61	*Alkaline phosphatase 1 (ALP1)*
RhiirDAOM197198_2|24357	-0.80	*EXS family phosphate transporter (PHO1)*
RhiirDAOM197198_2|14283	NA	*Pi:H+ symporter (RiPT4)*
RhiirDAOM197198_2|9790	-0.63	*Acid phosphatase 5-5 (ACP5-5)*

Figure 7: Host genotype-dependent regulation of *R. irregularis* gene expression. A) Differentially expressed *R. irregularis* genes (log2 fold change >1 or <-1, padj<0.05) in *crn* and R108 roots. B) Heatmap of genes involved in fungal N metabolism. C) Heatmap of genes involved in fungal P metabolism. Significance: ***adjusted p-value (padj)<0.05, **padj<0.01, *padj<0.05; if no symbol is shown, fungal gene expression does not significantly differ between host genotypes. Transcript data used to produce these heatmaps can be found in supplementary table 7. Data for the same Argininosuccinate synthase (*ASS*) gene is shown in panels A) and B); data for the same H+-transporting ATPase (*HA1*) gene is shown in panels A) and C).